Modulating TRADD to restore cellular homeostasis and inhibit apoptosis

Modulating TRADD to restore cellular homeostasis and inhibit apoptosis

06/21/2020

Daichao Xu[1, 2#], Heng Zhao[1#], Minzhi Jin[1], Hong Zhu[1], Bing Shan[2], Jiefei Geng[1], Slawomir A. Dziedzic[1], Palak Amin[1], Lauren Mifflin[1], Masanori Gomi Naito[1], Ayaz Najafov[1], Jing Xing[3], Lingjie Yan[2], Jianping Liu[4], Ying Qin[2], Xinqian Hu[1], Huibing Wang[1], Mengmeng Zhang[2], Vica Jean Manuel[1], Li Tan[2], Zhuohao He[2, 5], Zhenyu J. Sun[6], Virginia M. Y. Lee[5], Gerhard Wagner[7] and Junying Yuan[1*].

[1]Department of Cell Biology, Harvard Medical School, 240 Longwood Ave. Boston, MA 02115, USA;

[2]Interdisciplinary Research Center on Biology and Chemistry, Shanghai Institute of Organic Chemistry, Chinese Academy of Sciences, 26 Qiuyue Rd., Pudong, 201210 Shanghai, China;

[3]Department of Pediatrics and Human Development, Michigan State University, Grand Rapids, MI 49503, USA.

[4]State Key Laboratory of Bio-organic and Natural Products Chemistry, Shanghai Institute of Organic Chemistry, Chinese Academy of Sciences, 345 Lingling Rd., Xuhui, 200032 Shanghai, China;

[5]Center for Neurodegenerative Disease Research, Institute on Aging, Department of Pathology and Laboratory, University of Pennsylvania School of Medicine, Philadelphia, Pennsylvania 19104, USA.

[6]Department of Cancer Biology, Dana Farber Cancer Institute, 360 Longwood Avenue, Boston, MA 02215, USA;

[7]Department of Biochemistry and Molecular Pharmacology, Harvard Medical School, 240 Longwood Ave. Boston, MA 02115, USA;

Co-first authors listed in the alphabetical order of their last names.

*Corresponding author. Contact email address: junying_yuan@hms.harvard.edu

Abstract

Cell death in human disease is often a consequence of disrupted cellular homeostasis. Preventing cell death without restoring cellular homeostasis may lead to a persistent dysfunctional state that remains pathologically significant. While mechanisms of cell death have been thoroughly investigated[1-3], how to restore homeostasis after inhibition of cell death remains unclear. Here we identify TRADD[4-6], an adaptor protein, as a direct regulator of both cellular homeostasis and apoptosis. TRADD modulates cellular homeostasis by inhibiting TRAF2/cIAP1/2-mediated K63 ubiquitination of Beclin 1, thus reducing autophagy. TRADD deficiency inhibits RIPK1-dependent extrinsic apoptosis and proteasomal stress-induced intrinsic apoptosis. Furthermore, we identify small molecules ICCB-19 and Apt-1 that bind to a pocket on TRADD's N-terminal TRAF2 binding domain (TRADD-N) involved in interacting with TRADD-C and TRAF2 to modulate ubiquitination of RIPK1 and Beclin 1. Inhibition of TRADD by ICCB-19/Apt-1 blocks apoptosis and restores cellular homeostasis by activating autophagy in cells with accumulated mutant tau, α-synuclein, and Huntingtin. Treatment with Apt-1 restored proteostasis and inhibited cell death in a proteinopathy animal model induced by mutant Tau^{P301S}. We conclude that pharmacological targeting of TRADD may represent a promising strategy to inhibit cell death and restore homeostasis for treatment of human disease.

Short title: TRADD modulates cellular homeostasis and apoptosis

Main text

The accumulation of misfolded proteins in human disease promotes cell death and progressive pathology by disrupting cellular homeostasis[7]. Since the activation of autophagy is highly effective in reducing the accumulation of misfolded proteins and restoring cellular homeostasis[8,9], we sought to identify targets which could be manipulated pharmacologically to restore cellular homeostasis by inducing autophagy and inhibiting apoptosis simultaneously.

Inhibitors of apoptosis that can activate autophagy

No target is known which can simultaneously modulate autophagy and cell death; therefore, we designed and conducted a multiplexed cell-based screen to identify small molecule inhibitors of apoptosis mediated by proteasomal stress and RIPK1-dependent apoptosis (RDA) that can also activate autophagy (Extended Data Fig. 1a). This quadruplexed-screen of 170,000 compounds identified two active structural analogs, ICCB-17 and ICCB-19, and a close inactive analog, ICCB-19i (Fig. 1a). An SAR study identified an improved derivative Apostatin-1 (Apt-1). ICCB-19 and Apt-1 inhibited Velcade-induced apoptosis and RDA with IC50 ~1 μM (Extended Data Fig. 1b, c). Apt-1 showed no significant off-target activity on 97 kinases in KINOMEscan profiling (Extended Data Fig. 1d).

ICCB-19/Apt-1 effectively induced autophagy[10] (Fig. 1b, Extended Data Fig. 1e-i) and degradation of long-lived proteins[11] (Extended Data Fig. 1j). Caspase inhibitor zVAD.fmk had no effect on autophagy (Extended Data Fig. 1k). ICCB-19/Apt-1 had no effect on mTOR (Extended Data Fig. 1l). Rather, ICCB-19/Apt-1 treatment increased levels of DsRed-FYVE dots, an indicator for phosphatidylinositol-3-phosphate (PtdIns3P), a critical autophagy lipid messenger generated by the Atg14L-Beclin 1-Vps34-Vps15 class III PI3 kinase (PI3K-III) complex[12] (Extended Data Fig. 1m), suggesting the activation of PI3K-III complex. Consistently, treatment

with ICCB-19/Apt-1, but not ICCB-19i, increased Vps34 lipid kinase activity (Extended Data Fig. 1n). Treatment with Apt-1 increased interaction of Beclin 1 with TRAF2, cIAP1, and Atg14L, an important activator of Vps34 complex[13,14], but not with Vps34 (Fig. 1c, d; Extended Data Fig. 2a, b). ICCB-19/Apt-1-induced autophagy and long-lived protein degradation was significantly reduced by genetic or pharmacological inhibition of cIAP1/2 or TRAF2, which was rescued by cIAP1 and TRAF2 reconstitution, respectively (Fig. 1e, Extended Data Fig. 2c-h). Thus, ICCB-19/Apt-1-induced autophagy involves E3 ubiquitin ligases cIAP1/2 and adaptor TRAF2, which are not required for TORC1 inhibition or starvation-induced autophagy (Extended Data Fig. 2i-l). Treatment with ICCB-19/Apt-1, but not ICCB-19i, dramatically enhanced Beclin 1 K63 ubiquitination (Extended Data Fig. 2m). Apt-1-induced K63 ubiquitination of Beclin 1 was reduced by cIAP1/2 or TRAF2 deficiency and restored by reconstitution of cIAP1 or TRAF2, respectively (Fig. 1f, g; Extended Data Fig. 2n-p).

Mass spectrometry analysis identified conserved Beclin 1 K183 and K204 residues that may be modified by cIAP1 (Extended Data Fig. 3a-c). Double K183R/K204R mutant, but neither single mutant, reduced K63 ubiquitination of Beclin 1 mediated by cIAP1 (Extended Data Fig. 3d). Reconstitution of K183R/K204R double mutant, but neither single mutant, in Beclin 1 knockdown cells blocked induction of autophagy (Fig. 1h, Extended Data Fig. 3e-g) and reduced K63 ubiquitination of Beclin 1 induced by Apt-1 (Fig. 1i). Thus, Apt-1/ICCB-19 promote autophagy via K63 ubiquitination of Beclin 1 mediated by cIAP1/2 and TRAF2.

ICCB-19/Apt-1 indirectly inhibit RIPK1 kinase

The cleavage of caspase-3 induced by Velcade was blocked by ICCB-19/Apt-1, but not by Nec-1s[15] (Extended Data Fig. 4a, b). Like Nec-1s, ICCB-19/Apt-1 protected against multiple RDA models (Extended Data Fig. 4c-m), but not RIPK1-independent apoptosis (RIA) (Extended Data

Fig. 4n, o). ICCB-19/Apt-1 also partially inhibited necroptosis (Extended Data Fig. 4p, q). However, unlike Nec-1s, ICCB-19/Apt-1 cannot inhibit activation of overexpressed RIPK1 (Extended Data Fig. 4r). Thus, ICCB-19/Apt-1 are indirect inhibitors of RIPK1 kinase activity.

ICCB-19/Apt-1 target TRADD

TNFα stimulation promotes the formation of a transient intracellular complex (complex I) at TNFR1 which coordinates an intricate set of ubiquitination and phosphorylation events to control the activation of RIPK1, including both K63 ubiquitination mediated by TRAF2/cIAP1 and M1 ubiquitination mediated the LUBAC complex[16-19]. ICCB-19 treatment reduced the rapid activation of RIPK1 in complex I induced by TNFα (Fig. 2a), suggesting that the target of ICCB-19/Apt-1 may be a component of complex I. ICCB-19/Apt-1 treatment increased complex I recruitment of TRADD, HOIP, and A20, but not RIPK1, and also increased M1 ubiquitination but decreased K63 ubiquitination of RIPK1 (Fig. 2b, c, Extended Data Fig. 5a-c).

Since TRADD (Tumor necrosis factor receptor 1-associated DEATH domain), a 34 kDa adaptor with an N-terminal TRAF2 binding domain and C-terminal death domain, is the first protein recruited to complex I[4-6], TRADD may be the target for ICCB-19/Apt-1. *Tradd*$^{-/-}$ MEFs are known to be resistant to RDA[20]. Interestingly, in *Tradd*$^{-/-}$ MEFs Nec-1s, but not ICCB-19/Apt-1, offered additional protection against RDA (Fig. 2d, e). Thus, TRADD is required for protection of RDA by ICCB-19/Apt-1, but not Nec-1s.

In complex I, TRADD's N-terminal TRAF2-binding domain (TRADD-N) interacts with TRAF2 and cIAP1/2 to promote K63 ubiquitination of RIPK1[4,6,21,22]. Consistently, the protective effects of ICCB-19/Apt-1, but not Nec-1s, against RDA were reduced by genetic or pharmacological inhibition of cIAP1/2 and restored by cIAP1 reconstitution (Extended Data Fig. 5d-i). Thus, cIAP1/2-mediated ubiquitination is involved in ICCB-19/Apt-1's suppression of

RIPK1 activation. *Tradd*-knockout Jurkat cells were effectively protected against Velcade-induced apoptosis, which cannot be further enhanced by ICCB-19/Apt-1 (Fig. 2f). TRADD, but not FADD or RIPK1, are required for this protection (Extended Data Fig. 5j, k).

In *Tradd*$^{-/-}$ MEFs basal autophagic flux and long-lived protein degradation was increased relative to WT, which could not be further enhanced by ICCB-19/Apt-1 (Extended Data Fig. 6a-c). *Tradd*-knockout Jurkat cells also displayed increased levels of LC3 II, which was not altered by Apt-1 (Fig. 2g). Thus, TRADD is involved in inhibiting autophagy and required for ICCB-19/Apt-1-mediated induction of autophagy. Inhibition of autophagy by Spautin-1[23], *Atg5* knockout, or blocking lysosomal degradation prevented autophagy activation and protection against proteasomal stress-induced apoptosis in *Tradd* knockout or Apt-1-treated cells, but had no effect on RDA (Fig. 2g, Extended Data Fig. 6d-g).

Under homeostatic conditions, endogenous Beclin 1 bound to cIAP1/2 and TRAF2, which was enhanced by TRADD deficiency (Fig. 2h). Furthermore, K63 ubiquitination of Beclin 1 was enhanced in *Tradd*$^{-/-}$ MEFs, which was not affected by Apt-1, but could be suppressed by TRADD add-back, which was overcome by Apt-1 treatment (Fig. 2i; Extended Data Fig. 6h). These results suggest that ICCB-19/Apt-1 promote cIAP1/2/TRAF2-mediated K63 ubiquitination of Beclin 1 by releasing cIAP1/2/TRAF2 from TRADD.

ICCB-19/Apt-1 reduce inflammatory responses

Tradd$^{-/-}$ mice are normal and highly resistant to multiple systemic inflammatory responses[5,24-26]. Treatment with ICCB-19/Apt-1 minimally affected early events in the NF-κB pathway, but reduced production of TNFα-induced inflammatory target genes, NOS and COXII[27], and inflammatory cytokines in cells stimulated with pathogen-associated molecular patterns, including interferon γ (IFNγ), lipopolysaccharide (LPS), Pam3CSK4 (a synthetic bacterial lipopeptide), or

muramyl dipeptide (MDP) (Extended Data Fig. 7a-m). Consistently, WT mice treated with Apt-1 showed increased survival following intravenously-delivered TNFα, a murine model of systemic inflammation (Extended Data Fig. 7n, o).

ICCB-19/Apt-1 restore proteome homeostasis

We next investigated whether ICCB-19/Apt-1 could restore cellular homeostasis and promote degradation of misfolded proteins. Treatment with ICCB-19/Apt-1 reduced protein accumulation and cell death in the presence of Htt-103Q, WT, E46K, or A53T α-synuclein, and WT or P301L tau[28] (Extended Data Fig. 8a-f). PS19 mice, expressing mutant human P301S tau, develop progressive neuronal loss and microgliosis associated with neurofibrillary tangle (NFT)-like tau pathology[29]. Treatment with Apt-1 for 3 h induced autophagy and reduced the accumulation of mutant tau in cultured brain slices from PS19 mice, which was blocked by lysosomal inhibition (Extended Data Fig. 8g, h). Thus, Apt-1 can rapidly promote the degradation of accumulated mutant tau.

We tested the effect of Apt-1 in restoring proteostasis and reducing cell death in a mutant tau fibril (pff) transmission model[30]. Hippocampal delivery of Apt-1 (Extended Data Fig. 8i) was able to induce autophagy and reduce the levels of tau in these mice (Fig. 3a). Treatment with Apt-1 reduced NFT-like pathogenesis induced by pffs, including a reduction of hyperphosphorylated tau^+ neurons and pathological misfolded $MC1^+$ tau[31] (Fig. 3b, c). Tau pff-injected mice showed substantial increases in activated p-$RIPK1^+$ and apoptotic $TUNEL^+$ cells in the CA1 hippocampus, which was inhibited by Apt-1 (Fig. 3d, e). These results suggest that RIPK1 is activated in this tauopathy model and treatment with Apt-1 can effectively restore cellular homeostasis and block apoptosis driven by pathological tau transmission *in vivo*. Additionally, we tested whether Apt-1 could rescue proteostasis after NFT-like pathology had formed in PS19 mice. Apt-1 delivery for

one week was also able to reduce pre-formed NFT-like pathology in PS19 mice that were injected with Tau pff 3 weeks prior (Extended Data Fig. 8j, k).

ICCB-19/Apt-1 interact with TRADD-N

We found separately expressed TRADD-N (a.a.1-197) and TRADD-C (a.a.198-312) interacted, which was reduced by Apt-1 (Extended Data Fig. 9a), and thus, ICCB-19/Apt-1 might affect a previously unknown interaction of TRADD-N with TRADD-C. NanoBiT-based interaction between LgBiT-TRADD-N and TRADD-C-SmBiT was dose-dependently reduced by ICCB-19/Apt-1, but not ICCB-19i (Extended Data Fig. 9b-f). The direct binding of TRADD-N and TRAF2[21] was also reduced by Apt-1 in NanoBiT and FRET systems (Fig. 4a, Extended Data Fig. 9g-k). Thus, TRADD-N and TRADD-C normally interact with each other; in cells stimulated by TNFα, TRADD is recruited to TNFR1 mediated by the binding of its DD with the DD of TNFR1, which frees TRADD-N to interact with TRAF2 and organize complex I recruitment. Importantly, this model suggests that ICCB-19/Apt-1 might bind to a conserved interface on TRADD-N for binding to both TRADD-C and TRAF2. Consistently, Apt-1 increased the recruitment and retention of TRADD at TNFR1 and reduced TRADD binding to TRAF2/cIAP1, thus decreasing recruitment of TRAF2/cIAP1 to complex I (Fig. 4b, Extended Data Fig. 9l, m).

The addition of ICCB-19/Apt-1 to TRADD in a thermal shift assay[32] increased its Tm by 3.2°C and 3.7°C, respectively; ICCB-19i had no effect (Extended Data Fig. 10a-d). Incubation of Apt-1 with TRADD-N, but not TRADD-C, also increased Tm by 3.7°C (Fig. 4c, Extended Data Fig. 10e), suggesting that ICCB-19/Apt-1 likely bind TRADD-N. Saturation transfer difference (STD)-NMR[33] confirmed that ICCB-19/Apt-1, but not ICCB-19i, bind with TRADD-N (Extended Data Fig. 10f-h). Additionally, surface plasmon resonance (SPR) analysis determined binding K_D

of ICCB-19/Apt-1 with TRADD-N as 2.30 μM and 2.17 μM, respectively (Extended Data Fig. 10i, j, Fig. 4d).

We performed a ^{1}H-^{15}N heteronuclear single-quantum correlation NMR titration of Apt-1 with TRADD-N. The addition of Apt-1 into TRADD-N in solution significantly perturbed the following residues: Tyr16, Ala31, His34, Gln37, Ile72, Arg119, Gly121, Ala122, Arg124, and Arg146 (Extended Data Fig. 11a). The perturbed residues localized to β-sheets 1, 3, and 4, indicating that the interface comprised of these β-sheets mediates Apt-1 binding to TRADD-N. ICCB-19, but not ICCB-19i, exhibited similar binding on TRADD-N (Extended Data Fig. 11b, c).

NMR-based structures for ICCB-19/Apt-1 in binding with TRADD-N generated computationally showed that Apt-1/ICCB-19 bound with TRADD-N in similar conformations (Fig. 4e, Extended Data Fig. 11d). The ICCB-19/Apt-1 binding site is in the interface between TRADD-N and TRAF2-C[21]. TRADD-N residues Tyr16, Phe18, Ile72, and Arg119 form a hydrophobic pocket which can bind the substituted cycloheptane of ICCB-19/Apt-1. The amide group of Gly121 in TRADD-N forms a hydrogen bond with the carbonyl oxygen of ICCB-19/Apt-1. TRADD-N residues Gln142 and Asp145 form two hydrogen bonds with the heteroatoms of 4,5-dihydro-1H-imidazole group in ICCB-19. In addition, the phenyl group of Apt-1 forms π-π stacking with Tyr16. Consistently, binding of Apt-1 with recombinant TRADD-N mutants (Y16A, F18A, I72A, R119A, and G121A) was reduced relative to WT (Extended Data Fig. 11e, Fig. 4f).

Mutating TRADD-N Tyr16, Phe18, or Ile72 [21] reduced interaction with TRAF2-C (Extended Data Fig. 11f). G121A and A122T, but not R119A, reduced TRADD-N-TRAF2-C interaction. Expression of mutant TRADD Y16A, F18A, I72A, G121A, or A122T in *Tradd*-deficient cells did not suppress autophagy (Fig. 4g). TRADD R119A mutant suppressed autophagy, which was not overcome by Apt-1 (Fig. 4g). Consistent with a predicted H-bond between Gly121 and ICCB-19/Apt-1, Apt-1 could not further induce autophagy in G121A-TRADD-expressing *Tradd*-

knockout MEFs. In contrast, Apt-1 induced autophagy in A122T TRADD-N expressing *Tradd*-knockout cells (Fig. 4g). Thus, TRADD-TRAF2 interaction can regulate autophagy and furthermore, ICCB-19/Apt-1 interact with TRADD-N residues which mediate TRAF2-C binding[21]. Disrupting the interaction of TRADD and TRAF2 may recapitulate autophagy induction mediated by Apt-1/ICCB-19.

We also characterized the interaction of TRADD-N with TRADD-C in suppressing RDA. Compared to WT TRADD-N, the interactions of F18A, I72A, R119A, or G121A TRADD-N mutants with TRADD-C were all compromised (Extended Data Fig. 11g). *Tradd*-knockout cells complemented with Y16A, F18A, I72A, R119A, G121A, or A122T retained partial resistance to RDA (Extended Data Fig. 12a, b). Apt-1 was unable to provide additional protection in *Tradd*-knockout cells expressing G121A TRADD mutant and bound G121A TRADD-N with estimated K_D~274 μM (vs. K_D with WT TRADD-N = 2 μM) (Extended Data Fig. 12c-e). Apt-1 partially protected against RDA in *Tradd*-knockout cells complemented with Y16A, F18A, I72A, or R119A. The reconstitution of Y16A/F18A double-mutant or Y16A/I72A/R119A triple-mutant blocked RDA protection by Apt-1 (Extended Data Fig. 12f-h). Thus, the hydrophobic pocket formed by residues Tyr16, Phe18, Ile72, and Arg119 may collectively stabilize TRADD-N with ICCB-19/Apt-1.

Conclusion

TRADD is known to mediate extrinsic apoptosis by regulating RIPK1 activation in TNFR1 signaling[5,24-26]. Our study identifies that TRADD also regulates cellular homeostasis and intrinsic apoptosis mediated by proteasomal stress. ICCB-19/Apt-1 can bind with TRADD-N, disrupting its binding to both TRADD-C and TRAF2. ICCB-19/Apt-1 binding releases TRAF2/cIAP1/2 from TRADD to promote autophagy and diminish proteasomal stress by enhancing K63 ubiquitination

of Beclin 1. In RDA, ICCB-19/Apt-1 modulate TRADD to inhibit RIPK1 activation in complex I and decrease availability of TRADD to complex IIa to inhibit caspase activation (Extended Data Fig. 12i)[34]. Targeting TRADD would protect against inflammation and cell death mediated by both RIPK1-dependent and RIPK1-independent pathways as *Tradd* deficiency can protect against systemic inflammation and apoptosis in *Ripk1*$^{-/-}$ mice[35]. In conclusion, we identify TRADD as a novel therapeutic target, the first of its kind to both block cell death and inflammation and concurrently activate autophagy and restore cellular homeostasis.

Acknowledgement:

This work was supported in part by grants from UCB, FBRI-Fidelity, and the Quadrangle Fund for Advancing and Seeding Translational Research at Harvard Medical School (Blavatnik-Accelerator of Harvard and HMS/Q-FASTR) (to JY). The work of DX, LY, and BS during revision was supported in part by grants from the National Key R&D Program of China (2016YFA0501900), the China National Natural Science Foundation (31530041, 91849204 and 21837004), the Chinese Academy of Sciences (XDB39030000) and Shanghai Science and Technology Development Funds (20QA1411500). We thank Dr. Leslie Thompson of UC Irvine for Htt(Q103)-PC12 cells，Dr. Zhenggang Liu of NCI for *Tradd*$^{-/-}$ MEFs, Dr. Vishva Dixit of Genentech for M1 and K63 ubiquitin antibodies, and Dr. Peter Davies of Feinstein Institute for Medical Research for MC1 antibody. We thank Dr. Greg Cuny (University of Houston) for advice on chemistry, Dr. Zi-Fu Wang and Dr. Greg Heffron for advice on SPR and NMR, Dr. Jennifer Smith at the ICCB-Longwood for help with the compound screening, Dr. Jennifer Waters at the HMS Nikon microscope facility for help with microscopy, the EQNMR facility at HMS for their assistance and Drs. Chunxi Wang and Chunyang Cao (SIOC) for use of BIAcore.

Author contributions:

This project was conceived, designed, and directed by JY. DX and HZ designed and conducted majority of the experiments. MJ, HZ, JG, and SD conducted the multiplexed small molecule screen and contributed to early study of the compounds. ZJS and GW assisted with NMR analysis of TRADD/Apt-1 complex. JX conducted computational analysis of TRADD/Apt-1 complex. ZH and VL directed the tau transgenic mouse model study. YQ and LT synthesized ICCB-19 and 19i for revision. BS, PA, LM, MGN, AN, LY, JL, XH, HW, MZ, and VJM conducted some of the experiments. The manuscript was written by JY, DX, and HZ.

Competing interests

Authors claim no conflict of interest. Harvard has filed a patent on ICCB-19/Apt-1 series of small molecules.

Reference:

1 Wallach, D., Kang, T. B., Dillon, C. P. & Green, D. R. Programmed necrosis in inflammation: Toward identification of the effector molecules. *Science* **352**, aaf2154 (2016).

2 Shan, B., Pan, H., Najafov, A. & Yuan, J. Necroptosis in development and diseases. *Genes Dev* **32**, 327-340 (2018).

3 Ashkenazi, A. & Dixit, V. M. Death receptors: signaling and modulation. *Science* **281**, 1305-1308 (1998).

4 Hsu, H., Xiong, J. & Goeddel, D. V. The TNF receptor 1-associated protein TRADD signals cell death and NF-kappa B activation. *Cell* **81**, 495-504 (1995).

5 Pobezinskaya, Y. L. *et al.* The function of TRADD in signaling through tumor necrosis factor receptor 1 and TRIF-dependent Toll-like receptors. *Nat Immunol* **9**, 1047-1054 (2008).

6 Hsu, H., Shu, H. B., Pan, M. G. & Goeddel, D. V. TRADD-TRAF2 and TRADD-FADD interactions define two distinct TNF receptor 1 signal transduction pathways. *Cell* **84**, 299-308 (1996).

7 Sweeney, P. *et al.* Protein misfolding in neurodegenerative diseases: implications and strategies. *Transl Neurodegener* **6**, 6 (2017).

8 Morishita, H. & Mizushima, N. Diverse Cellular Roles of Autophagy. *Annu Rev Cell Dev Biol* **35**, 453-475 (2019).

9 Menzies, F. M. *et al.* Autophagy and Neurodegeneration: Pathogenic Mechanisms and Therapeutic Opportunities. *Neuron* **93**, 1015-1034, doi:10.1016/j.neuron.2017.01.022 (2017).
10 Yoshii, S. R. & Mizushima, N. Monitoring and Measuring Autophagy. *Int J Mol Sci* **18** (2017).
11 Zhao, J., Zhai, B., Gygi, S. P. & Goldberg, A. L. mTOR inhibition activates overall protein degradation by the ubiquitin proteasome system as well as by autophagy. *Proc Natl Acad Sci U S A* **112**, 15790-15797, doi:10.1073/pnas.1521919112 (2015).
12 Noda, T. & Yoshimori, T. Molecular basis of canonical and bactericidal autophagy. *International immunology* **21**, 1199-1204 (2009).
13 Zhong, Y. *et al.* Distinct regulation of autophagic activity by Atg14L and Rubicon associated with Beclin 1-phosphatidylinositol-3-kinase complex. *Nat Cell Biol* **11**, 468-476 (2009).
14 Matsunaga, K. *et al.* Two Beclin 1-binding proteins, Atg14L and Rubicon, reciprocally regulate autophagy at different stages. *Nat Cell Biol* **11**, 385-396 (2009).
15 Degterev, A. *et al.* Identification of RIP1 kinase as a specific cellular target of necrostatins. *Nat Chem Biol* **4**, 313-321 (2008).
16 Wertz, I. E. *et al.* Phosphorylation and linear ubiquitin direct A20 inhibition of inflammation. *Nature* **528**, 370-375, doi:10.1038/nature16165 (2015).
17 Haas, T. L. *et al.* Recruitment of the linear ubiquitin chain assembly complex stabilizes the TNF-R1 signaling complex and is required for TNF-mediated gene induction. *Mol Cell* **36**, 831-844 (2009).
18 Ofengeim, D. & Yuan, J. Regulation of RIP1 kinase signalling at the crossroads of inflammation and cell death. *Nat Rev Mol Cell Biol* **14**, 727-736 (2013).
19 Vucic, D., Dixit, V. M. & Wertz, I. E. Ubiquitylation in apoptosis: a post-translational modification at the edge of life and death. *Nat Rev Mol Cell Biol* **12**, 439-452 (2011).
20 Guo, X. *et al.* TAK1 regulates caspase 8 activation and necroptotic signaling via multiple cell death checkpoints. *Cell Death Dis* **7**, e2381 (2016).
21 Park, Y. C. *et al.* A novel mechanism of TRAF signaling revealed by structural and functional analyses of the TRADD-TRAF2 interaction. *Cell* **101**, 777-787 (2000).
22 Shu, H. B., Takeuchi, M. & Goeddel, D. V. The tumor necrosis factor receptor 2 signal transducers TRAF2 and c-IAP1 are components of the tumor necrosis factor receptor 1 signaling complex. *Proc Natl Acad Sci U S A* **93**, 13973-13978 (1996).
23 Liu, J. *et al.* Beclin1 controls the levels of p53 by regulating the deubiquitination activity of USP10 and USP13. *Cell* **147**, 223-234 (2011).
24 Chen, N. J. *et al.* Beyond tumor necrosis factor receptor: TRADD signaling in toll-like receptors. *Proc Natl Acad Sci U S A* **105**, 12429-12434 (2008).
25 Michallet, M. C. *et al.* TRADD protein is an essential component of the RIG-like helicase antiviral pathway. *Immunity* **28**, 651-661 (2008).
26 Ermolaeva, M. A. *et al.* Function of TRADD in tumor necrosis factor receptor 1 signaling and in TRIF-dependent inflammatory responses. *Nat Immunol* **9**, 1037-1046 (2008).
27 Callejas, N. A., Casado, M., Bosca, L. & Martin-Sanz, P. Requirement of nuclear factor kappaB for the constitutive expression of nitric oxide synthase-2 and cyclooxygenase-2 in rat trophoblasts. *J Cell Sci* **112 Pt 18**, 3147-3155 (1999).
28 Apostol, B. L. *et al.* Mutant huntingtin alters MAPK signaling pathways in PC12 and striatal cells: ERK1/2 protects against mutant huntingtin-associated toxicity. *Hum Mol Genet* **15**, 273-285 (2006).

29 Yoshiyama, Y. *et al.* Synapse loss and microglial activation precede tangles in a P301S tauopathy mouse model. *Neuron* **53**, 337-351 (2007).
30 Iba, M. *et al.* Synthetic tau fibrils mediate transmission of neurofibrillary tangles in a transgenic mouse model of Alzheimer's-like tauopathy. *J Neurosci* **33**, 1024-1037 (2013).
31 Jicha, G. A., Bowser, R., Kazam, I. G. & Davies, P. Alz-50 and MC-1, a new monoclonal antibody raised to paired helical filaments, recognize conformational epitopes on recombinant tau. *J Neurosci Res* **48**, 128-132 (1997).
32 Groftehauge, M. K., Hajizadeh, N. R., Swann, M. J. & Pohl, E. Protein-ligand interactions investigated by thermal shift assays (TSA) and dual polarization interferometry (DPI). *Acta Crystallogr D Biol Crystallogr* **71**, 36-44 (2015).
33 Cho, H. J. *et al.* Probing the effect of an inhibitor of an ATPase domain of Hsc70 on clathrin-mediated endocytosis. *Mol Biosyst* **11**, 2763-2769 (2015).
34 Micheau, O. & Tschopp, J. Induction of TNF receptor I-mediated apoptosis via two sequential signaling complexes. *Cell* **114**, 181-190 (2003).
35 Anderton, H. *et al.* RIPK1 prevents TRADD-driven, but TNFR1 independent, apoptosis during development. *Cell Death Differ* **26**, 877-889 (2019).
36 Voortman, J., Checinska, A. & Giaccone, G. The proteasomal and apoptotic phenotype determine bortezomib sensitivity of non-small cell lung cancer cells. *Mol Cancer* **6**, 73 (2007).
37 Cox, J. & Mann, M. MaxQuant enables high peptide identification rates, individualized p.p.b.-range mass accuracies and proteome-wide protein quantification. *Nat Biotechnol* **26**, 1367-1372, doi:10.1038/nbt.1511 (2008).

Methods

Animals

WT (Catalog No. 004781) and transgenic tauP301S (Catalog No. 008169) mice were from The Jackson Laboratory. All animals were maintained in a pathogen-free environment, and the animal experiments were conducted according to the protocols approved by the Harvard Medical School Institutional Animal Care and Use Committee (IACUC).

A multiplexed chemical screen

The primary screen was conducted in Jurkat cells treated with proteasomal inhibitor Velcade to induce apoptosis by proteasomal stress[36]. Inhibition of apoptosis by pan-caspase inhibitor zVAD.fmk was able to partially rescue cell survival, and thus was used as a positive control. ~170,000 compounds were screened to identify hits which could inhibit apoptosis induced by proteasomal stress better than that of zVAD.fmk. These positive hits were counter-screened

against apoptosis induced by 5-fluorouracil (5-FU) to remove generic inhibitors of DNA damage-induced apoptosis. Hits that protected against apoptosis induced by Velcade, but not 5-FU, were further evaluated for their ability to induce autophagy using H4-GFP-LC3 cells. Finally, the hits were further tested in RIPK1 dependent apoptosis (RDA) assay of extrinsic apoptosis in RGC5 mouse retinal ganglion cells treated with TNFα and 5z-7-Oxozeaenol (5z7, an inhibitor of TAK1).

Stereotaxic surgery and Apt-1 delivery

Intracranial injections of synthetic tau-preformed fibrils (pffs) into PS19 mice accelerate the transmission of pathological tau tangle-like aggregates throughout the brain and thus, provide a model for AD pathology and tauopathy[30]. Eight-week-old PS19 mice (P301S tau), expressing T34 isoform of human P301S mutant tau under the control of the mouse prion promoter, were deeply anesthetized with isoflurane and immobilized in a stereotaxic frame. The stereotaxic injections were made using predetermined coordinates with a Hamilton syringe under aseptic conditions. All injected animals were observed during and after surgery, and an analgesic was administered after surgery. T40/PS recombinant tau pffs (2 μg/μl) were injected into both sides of hippocampus of PS19 mice (ML, ±1.8 mm; AP, -2.2 mm; DV, 1.8 mm)[30]. The total volume injected 2.5 μl/injection for all mice. The mice were then either dosed immediately or waited for three weeks before delivering Apt-1 intracerebroventricularly via an ALZET micro-osmotic pump (ALZET Micro-Osmotic Model 1002). ALZET brain infusion kit was used for delivery into lateral ventricles (ML, -1.0 mm; AP, -0.5 mm; DV, 2.0 mm) at a rate of 0.25 μl/h. The ALZET micro-osmotic pumps were fixed on the skulls of the mice by instant adhesive and the skin incision was closed by suture. Apt-1 (20 mM) in the ALZET micro-osmotic pumps was renewed every two days and the Apt-1 delivery was maintained for a month in the immediate dosing groups or one week in the delayed dosing group. Apt-1 treatment resulted no apparent difference in survival or behavior of the mice. At the end of Apt-1 dosing for one month or one week, the mice were sacrificed and perfused by

PBS and the hippocampi from half of the brains were dissected and analyzed by immunoblotting after lysis in RIPA buffer (50mM Tris-HCl pH 7.5, 150mM NaCl, 1% NP-40, 0.1% SDS). The other half of the brains were fixed in 4% paraformaldehyde and embedded in paraffin blocks from which 5-μm-thick sections were processed for immunohistochemistry (IHC) using AT8 (specific for pathological tau phosphorylated at Ser202/Thr205, 1:10,000; Invitrogen), MC1 (specific for a pathological conformation of tau, 1:2000)[31] and TUNEL (terminal deoxynucleotidyl transferase dUTP nick end labeling).

Pharmacokinetic (DMPK) study of Apt-1

WT mice (2 months old) were deeply anesthetized with isoflurane and immobilized in a stereotaxic frame using predetermined coordinates under aseptic conditions. All animals were observed during and after surgery, and an analgesic was administered after surgery. Apt-1 (20 mM, 100 μl, release rate: 0.25 μl/h) was delivered intracerebroventricularly via an ALZET micro-osmotic pump (ALZET Model 1002) and ALZET brain infusion kits into lateral ventricles (ML, -1.0 mm; AP, -0.5 mm; DV, 2.0 mm). The ALZET micro-osmotic pumps were fixed on the skulls of the mice by instant adhesive and the skin incision was closed by suture. At 1h, 6h and 24h after the onset of delivery, cerebrospinal fluid (CSF) was carefully withdrawn by a Hamilton syringe from lateral ventricles (ML, -1.0 mm; AP, -0.5 mm; DV, 2.0 mm) for DMPK analysis. The mice were sacrificed at 24h and the hippocampi were dissected for DMPK analysis. The number of mice is 3 for each time point. The concentrations of Apt-1 in collected samples were measured by HPLC as a custom service by the Scripps Research Institute Florida.

Organotypic brain slice preparation

PS19 mice (4 months old) were anesthetized with isoflurane prior to decapitation. The brain was removed and immediately immersed in ice-cold cutting solution (2.5 mM KCl, 5 mM $MgCl_2$, 11 mM D-Glucose, 238 mM Sucrose, 26 mM $NaHCO_3$, 1mM NaH_2PO_4, 1 mM $CaCl_2$). The

cerebellum was trimmed off and the caudal end of the brain was glued onto the cutting table of the vibratome (LEICA VT1000 S, Germany). The brain was cut in coronal slices of 350 mm with an amplitude of 1.5 mm, a frequency of 75 Hz and a velocity of 0.1 mm/s. The slices were collected and stored in ice-cold cutting solution before floating onto semi-porous membrane inserts (Millipore, Millicell-CMLow Height Culture Plate Inserts, Schwalbach, Germany). Slices were cultured at 37 ˚C and 5% CO_2 in a culture medium consisting of 394 ml MEM, 10% normal horse serum, 5 mg/mL penicillin, 5 mg/mL streptomycin, 2.5ml L-glutamine, 1 mM $MgSO_4$, 11 mM D-Glucose, 238 mM Sucrose, 5 mM $NaHCO_3$, 1 mM $CaCl_2$, 26.6mM HEPES, 0.024ml 25% ascorbic acid and 0.5mg Insulin. Medium was changed every other day. Slices are maintained for 14 days *in vitro* prior to treatment.

Immunoblotting

Antibodies against the following proteins were used for western blot analysis: Atg14L (CST, 96752, 1:1000), HOIP (Abcam, ab46322, 1:1000), Vps34 (PTG, 12452-1-AP, 1:1000), LC3B (Sigma-Aldrich L7543, 1:1000), SQSTM1/p62 (CST 5114, 1:1000), α-Tubulin (Sigma-Aldrich T5168, 1:10000), Beclin-1 (CST 3738, 1:1000), phospho-RIPK1 (Ser166) (CST 31122, 1:1000), phospho-RIPK1 (Ser166) (Biolynx, BX60008-C3, 1:500 for IF), RIPK1 (D94C12, CST 3493, 1:1000), A20/TNFAIP3 (CST 4625, 1:1000), TRADD (Santa Cruz sc-7868, 1:500), TNF-R1 (CST 3736, 1:1000), β-Actin (Santa Cruz sc-81178, 1:5000), Caspase-3 (CST 9662, 1:1000), Cleaved Caspase-3 (CST 9661, 1:1000), TAU-5 (Invitrogen AHB0042, 1:1000), Phospho-Tau AT8 (Invitrogen MN1020, 1:1000), mouse cIAP1 (homemade, 1:1000), TRAF2 (CST 4724, 1:1000, Santa Cruz, sc-7346, 1:1000), Phospho-AMPKα (CST 2535, 1:1000), AMPKα (CST 2532, 1:1000), Phospho-Acetyl-CoA Carboxylase (CST 3661, 1:1000), Acetyl-CoA Carboxylase (CST 3662, 1:1000), Phospho-S6 (CST 2211, 1:1000), S6 (CST 2217, 1:1000), FADD (abcam ab124812, 1:1000), phospho MLKL (CST 91689, 1:1000), MLKL (CST 14993, 1:1000), phospho

RIPK3 (CST 57220, 1:1000), RIPK3 (CST 13526, 1:1000), Caspase-8 (CST 4790, 1:1000), PARP (CST 9542, 1:1000), GAPDH (CST 2118, 1:1000), phospho-IκBα (CST 9246, 1:1000), IκBα (CST 9242, 1:1000), phospho-IKKα/β (CST 2697, 1:1000), IKKβ (CST 2684, 1:1000), phospho-Erk1/2 (CST 9101, 1:1000), Erk1/2 (CST 9102, 1:1000), phospho-SAPK/JNK (CST 9251, 1:1000), SAPK/JNK (CST 9252, 1:1000), phospho-p38 MAPK (CST 9211, 1:1000), p38 MAPK (CST 9212, 1:1000), iNOS (CST 2982, 1:1000), Cox2 (CST 4842, 1:1000), Alpha-synuclein (abcam ab6162, 1:1000), Flag (Sigma-Aldrich F3165, 1:1000), HA (Sigma-Aldrich H6908, 1:1000), Beclin 1 (Santa Cruz, sc-48341, 1:100 for IP, CST, 3495, 1:1000), Atg5 (Abcam, ab108327, 1:1000). Anti-K63 Ub and anti-M1 Ub (a generous gift from Dr. Vishva Dixit, Genentech, 1:1000 for IP), anti-MC1 (a generous gift from Dr. Peter Davies, Feinstein Institute for Medical Research, 1:2000 for IHC). The signals were detected by Amersham ECL Western Blotting Detection Reagent (RPN2106, GE Healthcare), SuperSignal West Pico PLUS Chemiluminescent substrate (34580, Thermo) or SuperSignal West Femto Maximum Sensitivity substrate (34095, Thermo). The membranes were reprobed after incubation in Restore Western Blot stripping buffer (21063, Thermo).

Construction and transfection of plasmids

Full-length cDNAs for mouse/human TRADD were PCR-amplified from the plasmid library and cloned into pcDNA3.1 using Phanta Max Super-Fidelity DNA Polymerase (Vazyme Biotech Co., Ltd) with appropriate tags. Mutant hTRADD were generated using MutExpress II mutagenesis kit (Vazyme Biotech Co., Ltd). For protein purification, cDNA encoding truncated hTRADD (aa1-179, WT or mutant) were cloned into pET-28a plasmid for *E.coli* expression using ClonExpress II One Step Cloning Kit (Vazyme Biotech Co., Ltd), cDNA encoding GST-tagged hTRADD (Full length or aa180-312) was cloned into EcoRV/NotI sites in pEBG plasmid for mammalian expression, cDNAs encoding mVenus- and Flag-tagged TRADD-N(aa1-179) and mCerulean- and

Flag-tagged TRAF2-C (aa310-501) were cloned into pLenti plasmid for mammalian expression. All plasmids were verified by DNA sequencing and the details of the plasmid sequences are available upon request. Transient transfections of H4 and SH-SY5Y cells were performed using Lipofectamine 3000 (Invitrogen) according to the manufacturers' instructions. Briefly, cells were plated at a density of 5×10^{4} cells per well in a 12-well plate and transfected with a total of 1 μg DNA per well for 24 h. Medium was changed the day after transfection.

Generation of knockdown, knockout and reconstitution lines

Cells were stably infected with shRNA against mouse *Traf2* (TAGTTCGGCCTTTCCAGATAA), human *BECN1* 3'-UTR (CTCTGTGTTAGAGATATGA) or scramble control in the pLKO.1 lentiviral background. For CRISPR/Cas9 system-mediated gene knockout, guide RNA against human *Tradd*: sg*Tradd*-1 (GCGCGCAGCTCCAGTTGCAG), sg*Tradd*-2 (GCGCCCCCTCGCGGTAGGCG); *Atg5*: sg*Atg5*-1 (GCTTCAATTGCATCCTTAGA), sg*Atg5*-2 (GTGCTTCGAGATGTGTGGTT) in the Lenti-CRISPR v2 lentiviral background. Viral supernatant fractions were collected 48h after the transfection. Cleared supernatant fraction was filtered through a 0.45-mm filter. Polybrene (8 mg/ml) was supplemented to viral supernatant fractions. 24 h after infection, cells stably expressing shRNA or sgRNA were obtained by selection with 5 μg/ml puromycin. *BECN1* 3'-UTR shRNA expressing H4 cells were infected with lentiviral particles expressing Flag-Beclin 1 (WT or mutant). Polyclonal populations were screened until WT and mutant lines were generated that had near endogenous Beclin 1 reconstitution levels.

Analysis of cytotoxicity and viability

The rates of cell death were measured in triplicate or quadruplicate in a 96-well or 384-well plate by using SYTOX Green Nucleic Acid Stain (Invitrogen) or ToxiLight Non-destructive Cytotoxicity BioAssay Kit (Lonza). The intensity of luminescence was determined in an EnSpire Multimode Plate Reader (PerkinElmer). Data was collected by using PerkinElmer EnVision

Manager Version 1.13 software. Cytotoxicity is expressed as percentages of cell death per well after deducting the background signal in non-induced cells and compared to that of the maximal cell death with 100% Lysis Reagent. The rates of cell viability were determined by using CellTiter-Glo Luminescent Cell Viability Assay (Promega) following the manufacturer's protocol and the results are expressed as percentages of luminescence intensity per well after deducting the background signal in blank well and compared to that of the viability in the non-treated wells. Concentration of drugs used for inducing or inhibiting cell death, mTNFα: 1 ng/ml； 5Z-7-Oxozeaenol: 0.5 μM; Velcade: 50 nM; Apt-1/ICCB-19/ICCB-19i/Nec-1s: 10 μM.

Caspase-8 activity assay

Caspase-Glo 8 assay (Promega) was used to detect the activity of caspase-8 in cells and in vitro by following manufacture's protocol. Briefly, 2×10^5 cells (MEFs) were plated in 6-well plates and treated as indicated in 2 ml for the indicated times. After treatment, media was removed, and 300 μl 0.5% NP-40 lysis buffer (50 mM Tris-HCl pH 7.5, 150 mM NaCl and 0.5% NP-40) was added to each well, cells were scraped and lysates were left on ice for 5 min. 10 μl of lysate per condition were transferred into a 384-well plate and 90 μl of Caspase-Glo 8 reagent supplemented with MG-132 (30 μM) was added to each well. Plates were wrapped in foil and gently mixed using a plate shaker at 300-500rpm for 30 sec. Reactions was allowed to proceed by incubation at room temperature for 1h. Caspase-8 activity was read on a luminometer.

Complex-I/II purification

Cells were seeded in 15 cm dishes and treated as indicated with Flag-TNFα (50 μg/ml). To terminate treatment, media was removed and plates were washed with 50 mL of ice cold PBS. Plates were frozen at -80C until all time points were acquired. Plates were thawed on ice and cells were lysed in 0.5% NP-40 lysis buffer (50 mM Tris-HCl pH 7.5, 150 mM NaCl and 0.5% NP-40) supplemented with protease inhibitors and N-Ethylmaleimide (2.5 mg/ml). Cell lysates were

rotated at 4C for 30 min then clarified at 4C at 14,000 rpm for 30 min. Proteins were immunoprecipitated from cleared protein lysates with 20 µl of anti-Flag M2 beads (Sigma) with rotation overnight at 4C. 4×washes in 0.5% NP-40 buffer with N-Ethylmaleimide were performed, and samples eluted by boiling in 50 µl 1×SDS loading buffer. For complex-II purification cells were seeded in 10 cm dishes and treated as indicated using media containing TNFα (10 ng/ml) and zVAD (20 µM). Cells were lysed on ice in 0.5% NP-40 lysis buffer. Cell lysates were rotated at 4C for 30 min then clarified at 4C at 14,000 rpm for 10 min. 20 µl of protein G Sepharose (Sigma), after pre-blocking for 1h with lysis buffer containing 1% BSA, were incubated with FADD antibody (1.5 mg antibody/mg protein lysate) and the mixture was incubated in rotation with cleared protein lysates 4h at 4C. The samples were then washed four times in lysis buffer and eluted by boiling in 50 µl 1×SDS loading buffer. Concentration of compounds used in complex-I/II purification: 10 µM (Apt-1 or ICCB-19).

Long-lived protein degradation assay

H4 cells were cultured with L-[3,4,5-^{3}H(N)]-leucine (0.1 µCi/ml) (PerkinElmer Life Sciences) for 24h and chased in media with nonradioactive leucine for 18h. Then the media was changed and incubated for additional 6h along with different compounds (10 µM Apt-1, 10µ M ICCB-19, 10 µM ICCB-19i, 1 µM rapamycin). The media were recovered and treated with 10% trichloroacetic acid to separate trichloroacetic acid-soluble (amino acids) and trichloroacetic acid-insoluble (proteins) fractions. The cells were completely dissolved with 1N NaOH. Radioactivity was measured with a liquid scintillation analyzer (PerkinElmer). Long-lived protein degradation was calculated by dividing trichloroacetic acid-soluble radioactivity in the media by total radioactivity detected in the cells and media. The values were expressed as changes in fold from the value obtained in control cells.

NanoBiT protein-protein interaction (PPI) assay

The Nano-Glo Live Cell assay kit (Promega) was used as follows: HEK293T cells were seeded at 7.5×10^3 cells per well in a white, clear-bottom 96-well plate 12h before transfection (10 ng LgBiT-fused construct and 10 ng SmBiT-fused construct). After 24h incubation, medium was removed and replaced with 100 μl Opti-MEM medium for 1h at 37C. The Nano-Glo reagent was prepared as per manufacturer's instructions and added to each well immediately before the luminescence reading was taken. Luminescence was measured at 1 min intervals for 10 min on a plate reader and reported as relative light units (RLU). For quantitative comparison of LgBiT-SmBiT interactions, the peak values at the 2-3 min time point were used. Concentration of compounds used in NanoBiT assay: 10 μM (Apt-1, ICCB-19 or ICCB-19i).

Protein expression and purification

Recombinant WT and mutant His-TRADD-N (aa1-179) protein fragment was expressed in BL21 (DE3) *E. coli* after induction with 0.5 mM IPTG overnight at 16C. ^{15}N-labeled TRADD-N domain protein was purified from *E. coli* grown at 16C in minimal medium. Bacteria were harvested and disrupted by a high-pressure homogenizer and purified by Ni^{2+} affinity resin (GE Healthcare). All proteins were further purified by size exclusion chromatograph on a Superdex 75 column (GE Healthcare) in a buffer containing 20 mM imidazole (pH6.6), 200 mM NaCl, 20 mM DTT and 0.05% NaN_3. All NMR samples were in the same buffer at concentrations between 0.2-0.4 mM with 90% H_2O/10% D_2O. Proteins were exchanged into assay buffer (120 mM NaCl, 20 mM NaH_2PO_4/Na_2HPO_4, pH 7.4) by dialysis for thermal shift assay.

NMR spectroscopy

The ^{15}N-HSQC spectra of ^{15}N-labeled TRADD-N domain protein were acquired in a buffer containing 20 mM imidazole (pH6.6), 200 mM NaCl, 20 mM DTT and 0.05% NaN_3 at 25C, on a 600 MHz Bruker Avance II spectrometer using a Prodigy cryoprobe. For the spectra of 0.2 mM TRADD-N with 0.5 mM Apt-1 ligand, the data were collected with 8 number of scans for each

FID, 512 complex points in the direct ^{1}H dimension and 128 complex points in the indirect ^{15}N dimension. For the spectra of 0.4 mM TRADD-N with 0.5 mM ICCB-19, or 0.5 mM ICCB-19i, the data were collected with 2 number of scans for each FID, 512 complex points in the direct ^{1}H dimension and 128 complex points in the indirect ^{15}N dimension. The spectra were processed and analyzed using Bruker Topspin 3.6.1 software.

Saturation Transfer Difference-nuclear magnetic resonance (STD-NMR) spectroscopy [33] was used to detect the interaction of compounds with TRADD-N. The STD spectra were acquired on a 400 MHz spectrometer (ICCB-19 and Apt-1) or 800 MHz spectrometer (ICCB-19i). The samples for STD NMR were prepared as 13 μM TRADD-N or TRADD-N(G121A) with 1 mM Apt-1, ICCB-19 or ICCB-19i in 0.5 mL of PBS in D_2O (10%). The on-resonance irradiation was performed at a chemical shift of -0.5 ppm, whereas the off-resonance irradiation was conducted at 37 ppm. The spectra were acquired using the following parameters: spectral window of 6.4 kHz, number of scans at 320, acquisition time of 2 s, and repetition time of 3 s. The decrease in signal intensity in STD spectrum, resulting from the transfer of saturation from the protein to the ligand, is evaluated by subtracting the on-resonance spectrum from the off-resonance spectrum.

Thermostability shift assay

To determine stability, purified proteins were made to a final concentration of 1μg/μl. SYPRO Orange dye was added to the protein to make a final concentration of 2×. Compounds were added in the mix with a final concentration of 250 μM or as indicated and incubated at 4C for 1h. The experiments were performed in 384-well plates specific for real-time PCR instrument with a total volume of 20 μl/well. The assay plate was covered with a sheet of optically clear adhesive to seal each well. The assay plate was centrifuged at 800 × g for 2 min at 25C to collect solutions in the bottom of the well and remove bubbles. The assay plate was placed into the Applied Biosystems QuantStudio 6 Real-Time PCR System. The reaction was run from 25C, ramping up in increments

of 0.05°C/s to a final temperature of 95C with fluorescence detection throughout the experiment to generate a dataset. Melting temperature of the protein (Tm) was determined by performing non-linear fitting of the dataset to a Boltzmann Sigmoidal curve in GraphPad Prism with the following equation: Y=Bottom+(Top−Bottom)/[1+exp(Tm−X/Slope)], where Y= fluorescence emission in arbitrary units; X = temperature; Bottom = baseline fluorescence at low temperature; Top = maximal fluorescence at top of the dataset; Slope = describes the steepness of the curve, with larger values denoting shallower curves.

Surface plasmon resonance (SPR)

The binding affinity between ICCB-19/Apt-1 and TRADD-N was analyzed at 25C on a BIAcore T200 machine with CM5 chips (GE Healthcare). PBS-P buffer (GE Healthcare) was used for all measurements. For surface plasmon resonance (SPR) measurements, Flag-tagged TRADD-N protein was purified from HEK293T cells by anti-Flag affinity gel and eluted by 3×Flag peptide. The protein was further purified by size exclusion chromatograph on a Superdex 75 column (GE Healthcare) in a buffer containing 20 mM imidazole (pH 6.6), 200 mM NaCl, 20 mM DTT. The protein was dialyzed into PBS and diluted to a final concentration of 40 μg/ml in NaOAc buffer (pH 4.5) before immobilization on CM5 chip. ~5000 response units of protein were immobilized on the chip with a running buffer composed of PBS-P. Reference was used to normalize the response unit (RU) values of protein. A series of compound concentrations ranging from 0.3125 to 10 μM was tested at 30 μl/min flow rate. The contact time is 100 s and dissociation time is 120 s. When the data collection was finished in each cycle, the sensor surface was regenerated with PBS-P buffer. DMSO solvent correction was performed following the BIAcore T200 Guide. Binding curves were displayed, and equilibrium binding constants (K_D) for the interaction were determined using the steady-state affinity method incorporated in the BIAEVALUATION 4.1 software (GE Healthcare).

In vitro FRET assay

mVenus- and Flag-tagged TRADD-N (mVenus-TRADDN-Flag) and mCerulean- and Flag-tagged TRAF2C (Flag-TRAF2C-mCerulean) was expressed in HEK293T cells for 48h. Then cells were lysed in NP-40 buffer followed by immunoprecipitation using anti-Flag affinity gel. The proteins were eluted by 5 mg/ml 3×Flag peptide and exchanged into assay buffer (120 mM NaCl, 20 mM NaH_2PO_4/Na_2HPO_4, pH 7.4) by dialysis for FRET assay. The proteins were added into Corning black 96-well microtiter plates in triplicates at a final concentration of 1 μM. Apt-1 was incubated with the proteins for 1h before measurement. Measurements were performed on a fluorescent plate reader (Victor3, 1420 Multilabel counter, Perkin Elmer). The following filter set was used: mCerulean filter set (excitation: 430/15 nm, emission: 460/20 nm); mVenus filter set (excitation: 485/15, emission 535/15); FRET filter set (430/15 nm, emission 450-600 nm).

Mass spectrometry and data analysis

For complex I mass spectrometry analysis, MEFs were treated with Flag-TNFα in the presence or absence of ICCB-19 (10 μM) for indicated time. The binding proteins of TNFR1 in immunoprecipitation pulldown by anti-Flag-beads were trypsin digested. The peptides were analyzed on Q Exactive HF-X Hybrid Quadrupole-Orbitrap Mass Spectrometer (Thermo Scientific). Protein identification and quantification were performed by MaxQuant 1.2.1. The tandem mass spectra were searched against UniProt mouse protein database. The precursor and fragment mass tolerance were set as 20 ppm. The FDR at peptide spectrum match level and protein level was controlled below 1%. The unique peptides plus razor peptides were included for quantification.

For mass spectrometry analysis of ubiquitination sites of Beclin 1, Flag-tagged mBeclin 1 isolated from HEK293T cells expressing this construct was trypsin-digested on beads followed by immunoprecipitation. The resulting peptides were subjected to enrichment of diGly peptides using

antibody against ubiquitin remnant motif (K-ε-GG) (PTM Biolabs Inc). The enriched diGly peptides were analyzed on the Q Exactive HF-X mass spectrometer (Thermo Scientific). The identification and quantification of diGly peptides was done by MaxQuant. The tandem mass spectra were searched against UniProt mouse protein database together with a set of commonly observed contaminants. The precursor mass tolerance was set as 20 ppm, and the fragment mass tolerance was set as 0.1 Da. The cysteine carbamidomethylation was set as a static modification, and the methionine oxidation as well as lysine with a diGly remnant were set as variable modifications. The FDR at peptide spectrum match level was controlled below 1%.

The effect of Apt-1 on the binding partners of Beclin 1 was characterized by mass spectrometry. The proteins obtained by immunoprecipitation against Flag-tagged Beclin 1 in cells with or without Apt-1 treatment were trypsin digested. The resulting peptides in three replicates were analyzed on a Thermo Scientific Orbitrap Fusion Tribrid mass spectrometer. The protein identification and quantification were done by MaxQuant[37]. The tandem mass spectra were searched against the UniProt human protein database and a set of commonly observed contaminants. The precursor mass tolerance was set as 20 ppm, and the fragment mass tolerance was set as 0.5 Da. The cysteine carbamidomethylation was set as a static modification, and the methionine oxidation was set as a variable modification. The false discovery rate at the peptide spectrum match level and protein level was controlled to be <1%. The unique peptides plus razor peptides were included for quantification. The summed peptide intensities were used for protein quantification.

Molecular modeling and docking methods

The 3D atom coordinates of TRADD and TRAF2 interaction complex were obtained from PDB (https://www.rcsb.org) with PDB ID of 1F3V. The TRADD part of this 3D structure served as the protein receptor in the following induced-fit docking procedure performed with the molecular

simulation software suite Schrödinger (version 2018-1, Schrödinger, LLC, New York, NY, 2018). The receptor was first prepared with the Protein Preparation Wizard. The structure was preprocessed following default settings except no waters were deleted at this step, then hydrogen bond assignment and restrained minimization were performed in the refinement step, followed by removing the water molecules with less than 3 H-bonds to non-waters. The 3D structures of the small molecules were next prepared by LigPrep with no ionization but stereoisomers were generated. The prepared structures of TRADD receptor and small molecules were then submitted for induced-fit docking to predict the binding modes. At the beginning of this step, to define the binding site we inspected the interface of TRADD and TRAF2 interaction and set the docking pocket as the cavity around the center of residues Ile72, Ala122 and Arg146. Considering the surface residue flexibility, we specified refinement of the residues within 9 Å of the ligand during the induced-fit docking process.

Fluorescence microscopy

Cells were seeded at 2.5×10^4 cells per well on poly-L-lysine coated glass cover slips and transfected as described. Cells were fixed in 4% paraformaldehyde, followed by permeabilization with 0.1% Triton X -100. Nuclei were stained using DAPI (Sigma). Cells expressing GFP or RFP-fusion proteins were imaged with an Olympus Fluoview FV1000 confocal microscope (Olympus) using a 40×objective. Images were taken by using Olympus FV10-ASW 3.0 software. For GFP-LC3 and DsRed-FYVE puncta quantification, the average spot intensity in 1000 cells from each indicated sample was determined. Images were processed using ImageJ and Photoshop CC. Concentration of compounds used to induce or block autophagy: 10 μM (Apt-1, ICCB-19, ICCB-19i or Spautin-1), for 6 h or as indicated.

***In vivo* delivery of TNFα**

WT mice (n = 10, male, 8 weeks of age) were injected intravenously via the tail vein with mTNFα (9.5 μg/mouse) after an intraperitoneal injection of Apt-1 (20 mg/kg) 30 min before. Control mice (n=9) received an equal amount of vehicle 30 min before mTNFα challenge. Kaplan Meier survival curve was determined.

Vps34 lipid kinase assay

HEK293T cells were transfected with Flag-Beclin 1 for 18h and then treated with ICCB-19, ICCB-19i, Apt-1 (10 μM) for another 6h. Flag-Beclin 1 was immunoprecipitated by anti-Flag to isolate Beclin 1/Vps34 complex. Immunoprecipitated beads were added with sonicated phosphatidylinositol (1 μl of 5 mg) and ATP (1 μl of 10 mM) in 30 μl reaction buffer [40 mM Tris (pH 7.5), 20 mM $MgCl_2$, 1 mg/ml BSA] for 30 min at room temperature. Wortmannin (10 μM) was used as a control and added into the reaction to inhibit Vps34. The conversion of ATP into ADP levels was measured by an ADP-Glo Kinase Assay Kit (Promega) according to the manufacturer's instructions.

KINOMEscan profiling

KINOMEscan profiling was used to assess the interaction of Apt-1 with a panel of 97 kinases as a custom service (DiscoverX/Eurofins, San Diego, CA USA). Briefly, DNA-tagged recombinant kinases were produced in E. coli. The assay plates with kinases were incubated at room temperature with shaking for 1h and the affinity beads were washed with wash buffer (1× PBS, 0.05 % Tween 20). The beads were then re-suspended in elution buffer. The kinase concentration in the eluates was measured by qPCR. Apt-1 were screened at 10 μM, and the results for primary screen binding interactions are reported as % Ctrl, where lower numbers indicate stronger hits in the matrix.

Quantitative reverse-transcription PCR

Total RNA from skin tissue was extracted with Trizol reagent (Life Technologies) and RNeasy Columns (Qiagen) and cDNA was prepared with Superscript III cDNA-synthesis kit (Life Technologies). Quantitative reverse-transcription PCR of *Tnf* gene was performed with QuantStudio 6 Flex Real-Time PCR System (Applied Biosystems). Data was colleted by using QuantStudio 12K Flex software version 1.3 (Applied Biosystems). *Gapdh* was used as a reference gene. Data were analysed according to the ΔC_T method.

Quantification and statistical analysis

All cell death data are presented as mean ± s.d. of one representative experiment. Each experiment was repeated at least 3 times. Mouse data are presented as mean ± s.e.m. of the indicated n values. All immunoblots were repeated at least three times independently with similar results. Quantifications of immunoblots were performed by ImageJ 1.52a, the densitometry data are adjusted to loading control and normalized to control treatment. Error bars for immunoblot analysis represent the standard error of the mean between densitometry data from three unique experiments. Curve fitting and statistical analyses were performed with GraphPad Prism 8.0 or Microsoft Excel 2016 software, using either unpaired two-tailed Student's t-test for comparison between two groups, or one-way ANOVA with post hoc Dunnett's tests for comparisons among multiple groups with a single control, or two-way ANOVA with post hoc Bonferroni's tests for comparisons among different groups. Statistical comparisons for series of data collected at different time points were conducted by two-way ANOVA. Significance of *in vivo* survival data was determined by the two-sided log-rank (Mantel-Cox) test. Differences were considered statistically significant if $P < 0.05$(*); $P < 0.01$ (**); $P < 0.001$(***); and n.s., non-significant.

Data availability

The 3D atom coordinates of TRADD and TRAF2 interaction complex were obtained from PDB (https://www.rcsb.org) with PDB ID of 1F3V. Source data for all figure plots are provided with

the paper. The full gel blots and the proteomics data sets have been provided in the Supplementary Information. The data that support the findings of this study are available from the corresponding authors upon reasonable request.

Figure legends:

Figure 1. Identification of autophagy-activating inhibitors of both intrinsic and extrinsic apoptosis. **a**, Chemical structures of ICCB-17, ICCB-19, ICCB-19i, and Apt-1. **b**, Representative images and quantification of GFP-LC3 puncta in H4-GFP-LC3 cells treated as indicated. Mean ± s.e.m. of $n = 5$ biologically independent experiments. One-way ANOVA, post hoc Dunnett's test. **c**, Scatter plot depicting interactome changes of Beclin 1 from quantitative proteomics experiment. The targets are depicted as large red dots. **d**, Immunoprecipitation-immunoblot of MEFs. **e**, **h**, Immunoblot and quantification of LC3 II levels in MEFs of the indicated genotypes (**e**) or reconstituted H4 cells (**h**) treated with indicated compounds. Mean ± s.e.m. of $n = 3$ biologically independent experiments. **f**, **g**, K63 ubiquitination of Beclin 1 from MEFs of indicated genotypes treated with Apt-1. **i**, As in (**f**), using reconstituted H4 cells. Compounds treated at 10 μM, 6 h. For gel source data, see Supplementary Figure 1.

Figure 2. ICCB-19/Apt-1 require TRADD to block apoptosis and activate autophagy. **a**, **c**, RIPK1 ubiquitination and activation in MEFs treated with indicated compounds. **b**, Complex I was isolated and analyzed by mass spectrometry. Red dots: significant changes in ICCB-19-treated cells. Green/black dots: no change. **d**, **f**, Cell survival in MEFs (**d**) or Jurkat (**f**) of indicated genotypes treated with indicated compounds. Mean ± s.d. of $n = 3$ biologically independent samples. Two-way ANOVA, post hoc Bonferroni's tests (**d**, **f**). **e**, **g**, Immunoblot and quantification of CC3 (cleaved caspase-3) in MEFs (**e**) or LC3 II in Jurkat (**g**) of indicated genotypes treated with indicated compounds. Mean ± s.e.m. of $n = 3$ biologically independent experiments (**e**, **g**). **h**, Immunoprecipitation-immunoblot of Jurkat cells of indicated genotypes. **i**, K63 ubiquitination of Beclin 1 from control and reconstituted *Tradd*$^{-/-}$ MEFs treated with Apt-1. Compounds treated at 10 μM, 6 h or indicated. For gel source data, see Supplementary Figure 1.

Figure 3. ICCB-19/Apt-1 reduce neurofibrillary tangle-like tau inclusions and pathology induced by tau fibril transmission. **a-e**, Effects of Apt-1 on the pathological tangle-like tau aggregates in the hippocampus CA1 region of PS19 mice injected with tau pffs. Immunoblots of tau levels (**a**), immunostaining of phospho-tau (AT8) (**b**), p-RIPK1(S166) (**d**), TUNEL (**e**), and immunohistochemistry for tau in pathological conformation (MC1) (**c**) in hippocampus CA1 region. Each dot represents the mean from an individual mouse. Mean ± s.e.m. (n = 3). Two-tailed t-test. For gel source data, see Supplementary Figure 1.

Figure 4. The targeting mechanism of ICCB-19/Apt-1 on TRADD. a, The effect of Apt-1 on TRADD-N TRAF2-C binding by NanoBiT assay. Mean ± s.d. of n = 6 biologically independent samples. Two-tailed t-test. **b**, Immunoprecipitation-immunoblot and quantification (n = 1) of indicated protein in MEFs treated with Apt-1, representative of 3 independent experiments. **c**, **f**, *in vitro* binding of Apt-1 to His-TRADD-N WT and indicated mutants as determined by thermal shift assay. **d**, Kinetic profile of Apt-1 binding to TRADD-N from SPR analysis. **e**, Binding pose of Apt-1 in complex with TRADD-N generated by induced-fit docking. Left, shape and polarity of the ligand binding pocket surface (red, negatively charged; blue, positively charged). Right, details of the interaction. Apt-1 shown as cyan sticks, protein shown as pink cartoon with key residues highlighted in sticks. Dashed lines represent hydrogen bonds. **g**, Immunoblot and quantification of LC3 II in reconstituted *Tradd*$^{-/-}$ MEFs treated with Apt-1. Mean ± s.e.m. of n = 3 biologically independent experiments. Two-way ANOVA, post hoc Bonferroni's tests. Compounds treated at 10 μM, 6 h. For gel source data, see Supplementary Figure 1.

Extended Data Figure legends:

Extended Data Figure 1. Isolation of ICCB-19 and Apt-1 for modulating both apoptosis and autophagy. a, A multiplex chemical screening scheme for compounds that can modulate cellular homeostasis by activating autophagy and also block apoptosis. Primary screen: Jurkat cells were treated with Velcade (50 nM) and individual compounds (10 μM) in the library for 25h and cell viability was measured. 710 compounds which could protect against Velcade-induced apoptosis were selected. Secondary counterscreen: HCT116 cells were treated with 5-fluorouracil (5-FU) (100 μM) and individual compounds selected from the Primary screen (10 μM) for 24 h and cell viability was measured. The hits which protected against apoptosis induced by 5-FU were eliminated from further studies. Tertiary screen: H4-GFP-LC3 cells were treated with individual compounds (10 μM) for 24 h and GFP-LC3 dots were quantified. Quaternary screen: RGC-5 cells were treated with mTNFα (0.5 ng/ml), TAK1 inhibitor (5Z)-7-Oxozeanol (0.5 μM) and individual compounds (10 μM) for 8 h and cell viability was measured. **b**, IC50s of ICCB-19 and Apt-1 protecting Velcade-induced apoptosis (50 nM) in Jurkat cells treated with indicated compounds for 24 h and cell viability was measured. Mean ± s.d. of $n = 3$ biologically independent samples, representative of 3 independent experiments. **c**, IC50s of ICCB-19 and Apt-1 protecting RDA in MEFs were treated with mTNFα (1 ng/mL) and 5Z-7-Oxozeaenol (0.5 μM) in the presence of indicated compounds at different concentrations for 8 h and cell survival was measured. Mean ± s.d. of $n = 3$ biologically independent samples, representative of 3 independent experiments. **d**, KINOMEscan profiling of Apt-1 (10 μM) against a panel of 97 kinases. Binding interactions reported as % Ctrl, where lower numbers indicate stronger hits. Negative control = DMSO (100% Ctrl); positive control = control compound (0% Ctrl); $0 \leq$ %Ctrl < 0.1 Very Strong; $0.1 \leq$ %Ctrl $<$ 1 Strong; $1 \leq$ %Ctrl < 10 Medium; $10 \leq$ %Ctrl < 35 Weak; %Ctrl ≥ 35 No effects. No significant binding of Apt-1 to this panel of 97 kinases was detected. **e**, H4 cells were treated with indicated concentrations of Apt-1. Autophagy was determined by LC3 II levels using immunoblotting. SE

= shorter exposure, LE = longer exposure. Mean ± s.e.m. of n = 3 biologically independent experiments. **f-i**, SH-SY5Y (**f**), HeLa (**g**), HT-29 (**h**), and Jurkat (**i**) cells were treated with Apt-1 (10 μM), NH_4Cl (20 mM) as indicated for 6 h. Autophagy was measured by LC3 II induction and p62 reduction by immunoblotting. The levels of LC3 II in cells treated with both Apt-1 and NH_4Cl, the latter of which inhibits lysosome, were higher than that treated with either Apt-1 or NH_4Cl alone. Thus, ICCB-19/Apt-1, but not ICCB-19i, induce autophagic flux. Mean ± s.e.m. of n =3 independent experiments. Two-tailed t-test. $^{**}P$ = 0.0037 (**f**), 0.0024 (**g**), 0.0027 (**h**), 0.0036 (**i**). **j**, Effects of ICCB-19/Apt-1 on long-lived protein degradation. The rates of long-lived protein turnover in H4 cells treated with indicated compounds (10 μM, 6 h); rapamycin as positive control. Values expressed as fold changes relative to normal control cells. Mean ± s.e.m. of n = 4 biologically independent samples. One-way ANOVA, post hoc Dunnett's test. **k**, MEFs and Jurkat cells treated with zVAD.fmk (20 μM) for 6 h.Levels of LC3 II determined by immunoblotting. **l**, MEFs were treated with vehicle (0 h), ICCB-19 (10 μM), or Apt-1 (10 μM) for indicated times. Cell lysates analyzed by immunoblotting using indicated antibodies. **m**, H4-DsRed-FYVE cells were treated with indicated compounds for 6 h and imaged; representative cells shown. Average DsRed-FYVE puncta per 1000 cells from each sample was determined using ImageJ. Mean ± s.e.m. of the puncta per cell from n = 5 biologically independent experiments. One-way ANOVA, post hoc Dunnett's test. $^{**}P$ = 0.0034; $^{***}P$ = 0.0004; n.s. not significant (P = 0.6502). **n**, Beclin 1/Vps34 kinase complex isolated from Flag-Beclin 1 transfected HEK293T cells treated with ICCB-19, Apt-1, or ICCB-19i (10 μM) for 6 h. PI3P kinase activity was measured by *in vitro* lipid kinase assay using ADP-Glo Kinase Assay Kit. Wortmannin (10 μM) was used as a control to inhibit Vps34 kinase activity. Mean ± s.e.m. of n = 4 biologically independent samples. One-way ANOVA, post hoc Dunnett's tests. $^{***}P$ = 0.0003; 1×10^{-15} (left to right). For gel source data, see Supplementary Figure 1.

Extended Data Figure 2. cIAP1/2 and TRAF2 are required for induction of autophagy by ICCB-19/Apt-1. a, HEK29T cells were transfected with Flag-Beclin 1 for 12 h, then treated with Apt-1 (10 μM) for another 12 h. Cell lysates were immunoprecipitated using anti-Flag beads. cIAP1 and TRAF2 levels were determined by immunoblotting. **b**, MEFs were treated with indicated concentrations of Apt-1 for 12 h. Cell lysates were immunoprecipitated using anti-Beclin 1 antibody. cIAP1 and TRAF2 levels were determined by immunoblotting. **c**, **d**, Long-lived protein turnover rates in MEFs with indicated genotypes treated with indicated compounds. Expressed as fold changes relative to normal control cells. Mean ± s.d. of $n = 4$ biologically independent samples, representative of 3 independent experiments. Two-way ANOVA, post hoc Bonferroni's tests. $^{***}P = 3 \times 10^{-14}$, 6×10^{-10}, 1×10^{-7}, 2×10^{-8} (left to right, **c**, **d**). **e**, MEFs were pre-treated with SM-164 (1 μM) for 1 h, then treated with Apt-1 for 6 h. LC3 II levels were determined by immunoblotting. Mean ± s.e.m. of $n = 3$ biologically independent experiments. Two-tailed t-test. $^{***}P = 0.0003$. **f**, shRNA-mediated TRAF2 stable knockdown MEFs were treated with Apt-1 (10 μM) for 6 h. LC3 II levels were determined by immunoblotting. Mean ± s.e.m. of $n = 3$ biologically independent experiments. Two-tailed t-test. $^{**}P = 0.0012$. **g**, **h**, *cIap1*$^{-/-}$ and *Traf2*$^{-/-}$ MEFs reconstituted with HA-mcIAP1 and HA-mTRAF2, respectively, were treated with Apt-1 (10 μM) for 6 h. LC3 II levels were determined by immunoblotting. Mean ± s.e.m. of $n = 3$ biologically independent experiments. Two-tailed t-test$^{**}P = 0.0057$ (**g**), $^{***}P = 0.0007$ (**h**). **i**, **j**, MEFs with indicated genotypes were treated with rapamycin (1 μM) for indicated time. LC3 II levels were determined by immunoblotting. The quantification of each experiment was shown on the right ($n = 1$), representative of 3 independent experiments. **k**, **l**, MEFs with indicated genotypes were incubated in HBSS for indicated time. LC3II levels were determined by immunoblotting. The quantification of each experiment was shown on the right ($n = 1$), representative of 3 independent experiments.

m, MEFs were treated with indicated compounds for 6 h, then cell lysates were tandem-immunoprecipitated with anti-Beclin 1 antibody and denatured in 3 M urea. Anti-K63-linkage specific polyubiquitin antibody was used to conduct secondary immunoprecipitation. Samples were then immunoblotted with anti-Beclin 1 antibody to measure the K63-linkage specific ubiquitination of Beclin 1. **n**, MEFs were pretreated with SM-164 (1 μM) for 1 h, then treated with Apt-1 (10 μM) for 6 h, then K63-linkage specific ubiquitination of Beclin 1 was analyzed as in (**m**). **o**, **p**, Reconstituted MEFs were treated with Apt-1 (10 μM) for 6 h, then K63-linkage specific ubiquitination of Beclin 1 was analyzed as in (**m**). For gel source data, see Supplementary Figure 1.

Extended Data Figure 3. cIAP1 mediates K63 ubiquitination of Beclin 1 at K183 and K204. **a**, Schematic representation of mass spectrometry assay to determine K63 ubiquitination sites of Beclin 1 by cIAP1. **b**, The quantitative mass spec analysis of K63 ubiquitination of each lysine site. **c**, Sequence alignment of key ubiquitination sites (K) within Beclin 1 orthologs from different species. **d**, HEK293T cells were transfected with indicated plasmids for 24 h. Cells were lysed in 6 M urea and lysates were subjected to pull-down with Ni^{2+} beads and analyzed by immunoblotting with anti-Beclin 1 antibody to detect ubiquitylated Beclin 1. **e**, Validation of Beclin 1 expression in Beclin 1-silenced H4 cells. **f**, Control and Beclin 1-silenced H4 cells were treated with Apt-1 (10 μM) for 6 h. LC3 II levels were determined by immunoblotting. **g**, Beclin 1-silenced H4 cells reconstituted with WT and mutants Beclin 1 were treated with Apt-1 (10 μM) for 6 h. LC3 II levels were determined by immunoblotting. Mean ± s.e.m. are quantified from n = 3 biologically independent experiments in graphs. Two-tailed t-test. $^{**}P$ = 0.0022 (**d**), 0.0049 (**f**), 0.0024 (**g**); $^{*}P$ = 0.0309, 0.0195 (left to right, **d**), 0.0126 (**g**); n.s. not significant, (P = 0.6959) (**f**). For gel source data, see Supplementary Figure 1.

Extended Data Figure 4. ICCB-19/Apt-1 block Velcade-induced apoptosis, RIPK1-dependent apoptosis and necroptosis. a, **b**, Jurkat (**a**) or SH-SY5Y (**b**) cells were stimulated by Velcade (50 nM) in the presence of Apt-1 (10 μM), Nec-1s (10 μM), or zVAD (20 μM) for 12 h and 24 h. The levels of cleaved caspase-3 were determined by immunoblotting. **c**, *Tak1*$^{-/-}$ MEFs were treated with 1 ng/ml mTNFα in the presence of indicated compounds for 3 h. Mean ± s.d. of n = 3 biologically independent samples, representative of 3 independent experiments. One-way ANOVA, post hoc Dunnett's tests. $^{***}P = 1 \times 10^{-15}$ (left to right); n.s. not significant, ($P = 0.7989$). **d**, *Tak1*$^{-/-}$ MEFs were treated as in (**a**), the cell lysates were analyzed by immunoblotting using indicated antibodies. **e**, MEFs were treated with mTNFα (1 ng/ml) and 5Z-7-Oxozeaenol (0.5 μM) in the presence of indicated compounds for 1 h and 2 h and the cell lysates were analyzed by immunoblotting using indicated antibodies. **f**, **g**, ICCB-19/Apt-1 inhibit RDA, including complex IIa formation (**f**) and caspase-8 activation (**g**). MEFs treated as in (**e**) were lysed with IP buffer and FADD was immunoprecipitated by anti-FADD antibody. Total lysates and IP samples were analyzed by immunoblotting to determine the recruitment of RIPK1 to FADD in complex IIa (**f**). MEFs were treated with mTNFα (1 ng/ml) and 5Z-7-Oxozeaenol (0.5 μM) in the presence of ICCB-19 (10 μM), Apt-1 (10 μM), Nec-1s (10 μM), or zVAD.fmk (20 μM) for 4 h and the activity of caspase-8 was determined using Caspase-Glo 8 Assay Systems (**g**). Mean ± s.d. of n = 3 biologically independent samples, representative of 3 independent experiments. One-way ANOVA, post hoc Dunnett's tests. $^{***}P = 1 \times 10^{-15}$ (**g**). **h**-**k**, RDA was induced in *Tbk1*$^{-/-}$ MEFs (**h**, **i**), *Nemo*$^{-/-}$ MEFs (**j**, **k**) by the treatment with mTNFα (10 ng/ml) together with ICCB-19 (10 μM) and Nec-1s (10 μM) at indicated times and cell death was determined by SYTOX Green (**h**, **j**) and caspase-3 cleavage (CC3) immunoblotting (**i**, **k**). Mean ± s.d. of n = 3 biologically independent samples, representative of 3 independent experiments (**h**, **j**).). Two-way ANOVA. $^{***}P = 5 \times 10^{-7}$

(**h**), 4×10^{-7} (**j**). **l**, RDA was induced in WT MEFs by the treatment with mTNFα (10 ng/ml) and IKK inhibitor TPCA-1 (5 μM) in the presence of ICCB-19 (10 μM) or Nec-1s (10 μM) for indicated times and cell death was determined by SYTOX Green. Mean ± s.d. of $n = 3$ biologically independent samples, representative of 3 independent experiments. Two-way ANOVA. $^{***}P = 1 \times 10^{-5}$. **m**, Recombinant active caspase-8 was incubated with vehicle, ICCB-19 (10 μM), Apt-1 (10 μM), or zVAD.fmk (20 μM) for 1h and the activity of caspase-8 was determined using Caspase-Glo 8 Assay Systems. Mean ± s.d. of $n = 3$ biologically independent samples, representative of 3 independent experiments. One-way ANOVA, post hoc Dunnett's tests. n.s. not significant, (P = 0.9931, 0.9215 (left to right)). **n**, WT MEFs were treated with mTNFα (1 ng/ml) and cycloheximide (CHX, 1 μg/mL) to induce RIA in the presence or absence of ICCB-19 (10 μM) or Nec-1s (10 μM) for indicated time and cell survival was determined by CellTiter-Glo assay. Mean ± s.d. of $n = 8$ biologically independent samples, representative of 3 independent experiments. One-way ANOVA, post hoc Dunnett's tests. n.s. not significant, (P = 0.9962). **o**, p65/p50 DKO MEFs were treated with mTNFα (1 ng/ml) together with ICCB-19 (10 μM) for indicated times and cell survival was determined by CellTiter-Glo assay. Mean ± s.d. of $n = 3$ biologically independent samples, representative of 3 independent experiments. Two-way ANOVA. n.s. not significant, (P = 0.1895). **p**, MEFs were treated as indicated and the cell survival was measured by CellTiter-Glo assay. The concentrations of reagents used: mTNFα: 1 ng/mL; (5Z)-7-oxozeaenol: 0.5 μM; zVAD: 20 μM; ICCB-19: 10 μM; Apt-1: 10 μM; Nec-1s: 10 μM. Mean ± s.d. of $n = 3$ biologically independent samples, representative of 3 independent experiments. **q**, Necroptosis of MEFs was induced by the treatment with TNFα/5z7/zVAD in the presence of indicated compounds for indicated hours and the activation of RIPK1(p-S166), RIPK3(p-T231/S232), and MLKL(p-S345) was determined by immunoblotting. **r**, HEK293T cells were transfected with Flag-RIPK1 expression construct for 12 h in the presence of Nec-1s (10 μM), ICCB-19 (10 μM),

or Apt-1 (10 μM). The activation of RIPK1 was determined by immunoblotting using p-RIPK1(S166) antibody. For gel source data, see Supplementary Figure 1.

Extended Data Figure 5. The protection of RDA by ICCB-19/Apt-1 requires TRADD. a, **b**, Mass spectrometry analysis shown in Figure 2b using ICCB-19 (**a**) or Apt-1 (**b**) were confirmed by immunoprecipitation-immunoblotting using indicated antibodies, quantified on the right (n = 1), representative of 3 independent experiments. **c**, MEFs were treated with Flag-mTNFα (50 ng/ml) in the presence of Apt-1 (10 μM) for indicated time. The complex I was isolated by anti-Flag beads and denatured in 6 M urea. The complex I was further analyzed by immunoprecipitation using anti-M1 (6 M urea) or K63 (3 M urea) ubiquitin antibody under denatured condition. The levels of RIPK1 ubiquitination were analyzed by immunoblotting. **d**, WT and *Traf2*$^{-/-}$ MEFs were stimulated by mTNFα (1 ng/ml) and 5Z-7-Oxozeaenol (0.5 μM) in the presence of indicated compounds for 8 h. Cell survival was determined by CellTiter-Glo assay. Mean ± s.d. of n = 4 biologically independent samples, representative of 3 independent experiments. Two-way ANOVA, post hoc Bonferroni's tests. $^{***}P$ = 0.0001. **e**, WT and *cIap1/2*$^{-/-}$ MEFs were stimulated by mTNFα (10 ng/ml) in the presence of vehicle, ICCB-19 (10 μM) or Nec-1s (10 μM) for indicated time. Cell death was determined by CellTiter-Glo assay. Mean ± s.d. of n = 4 biologically independent samples, representative of 3 independent experiments. Two-way ANOVA. **f**, MEFs were pretreated with SM-164 (50 nM) for 1 h, then stimulated by mTNFα (10 ng/ml) in the presence of vehicle, ICCB-19 (10 μM) or Nec-1s (10 μM) for indicated time. Cell death was determined by SYTOX Green assay. Mean ± s.d. of n = 3 biologically independent samples, representative of 3 independent experiments. Two-way ANOVA. $^{***}P = 4 \times 10^{-5}$; n.s. not significant, (P = 0.1772). **g**, *cIap1/2*$^{-/-}$ MEFs were stimulated with Flag-TNFα (50 ng/ml) for indicated minutes in the presence of vehicle or ICCB-19 (10 μM) and the complex I was pulled

down using anti-Flag beads. The levels of activated RIPK1 and total RIPK1 were determined by immunoblotting. **h**, **i**, *cIap1/2*$^{-/-}$ MEFs (**h**) and cIAP1-reconstituted cIAP1/2 DKO MEFs (**i**) were stimulated with Flag-TNFα (50 ng/ml) for indicated minutes in the presence of vehicle or Apt-1 (10 μM) and the complex I was pulled down using anti-Flag beads. TRADD recruitment to complex I was determined by immunoblotting, quantified on the right (n = 1), representative of 3 independent experiments. **j**, **k**, *Fadd*-deficient and *Ripk1*-deficient Jurkat cells were treated with Velcade (50nM) in the presence of ICCB-19 (10 μM), Nec-1s (10 μM), NAC (100 μM), or zVAD.fmk (20 μM). The activation of caspase-8, PARP cleavage (**j**), and activation of caspase-3 (**k**) were determined by immunoblotting. For gel source data, see Supplementary Figure 1.

Extended Data Figure 6. Autophagy is required for ICCB-19/Apt-1 to inhibit Velcade-induced apoptosis. a, *Tradd*$^{+/+}$ and *Tradd*$^{-/-}$ MEFs were treated with vehicle or ICCB-19 (10 μM) for 6 h. Autophagy levels were determined by immunoblotting using anti-LC3 antibody. Mean ± s.e.m. of n = 3 biologically independent experiments (right). Two-tailed t-test. n.s. not significant, (P = 0.9172). **b**, *Tradd*$^{+/+}$ and *Tradd*$^{-/-}$ MEFs were treated with Apt-1 (10 μM), NH_4Cl (10 mM) as indicated for 6 h. Autophagy levels were determined by immunoblotting using anti-LC3 antibody. Mean ± s.e.m. of n = 3 biologically independent experiments. Two-tailed t-test. n.s. not significant (P = 0.4064, 0.8913 (left to right)). **c**, Long-lived protein turnover rates in *Tradd*$^{+/+}$ and *Tradd*$^{-/-}$ MEFs. Expressed as as fold changes relative to *Tradd*$^{+/+}$ cells. Mean ± s.e.m. of n = 5 biologically independent samples, representative of 3 independent experiments. Two-tailed t-test. $^{***}P$ = 0.0001. **d**, WT and *Tradd*-KO Jurkat cells were treated with Apt-1 (10 μM) and Spautin-1 (10 μM) followed by Velcade (50 nM) for 24 h. Cell survival was determined by CellTiter-Glo assay. Mean ± s.d. of n = 4 biologically independent samples, representative of 3 independent experiments. Two-way ANOVA, post hoc Bonferroni's tests. $^{***}P = 2 \times 10^{-5}$, 3×10^{-15} (left to right). **e**, Jurkat

cells were treated with ICCB-19 (10 μM), Apt-1 (10 μM), Chloroquine (50 μM), E64d (5 μg/ml) followed by Velcade (50 nM) for 24 h. The cell survival was determined by CellTiter-Glo assay. Mean ± s.d. of n = 4 biologically independent samples, representative of 3 independent experiments. Two-way ANOVA, post hoc Bonferroni's tests. $^{***}P = 4 \times 10^{-14}$, 1×10^{-15} (left to right). **f**, *Atg5*-WT and *Atg5*-KO Jurkat cells were pretreated with Apt-1 (10 μM) or zVAD (20 μM) for 1 h, then stimulated by Velcade (50 μM) for 24 h. Cell survival was determined by CellTiter-Glo assay. Mean ± s.d. of n = 4 biologically independent samples, representative of 3 independent experiments. Two-way ANOVA, post hoc Bonferroni's tests. $^{***}P = 1 \times 10^{-15}$. Validation of Atg5 knockout was determined by immunoblotting and shown on the right. **g**, $Atg5^{+/+}$ and $Atg5^{-/-}$ MEFs were stimulated by TNFα (1 ng/ml) and 5z7 (0.5 μM) for 8 h in the presence or absence of Apt-1 (10 μM). Cell survival was determined by CellTiter-Glo assay. Mean ± s.d. of n = 4 biologically independent samples, representative of 3 independent experiments. Two-way ANOVA, post hoc Bonferroni's tests. n.s. not significant, (P = 0.2568, 0.0822 (left to right)). **h**, HEK293T cells were transfected with indicated expression plasmids for 24 h. The whole-cell lysate lysed in 6 M urea was subjected to pull-down with Ni^{2+} beads and analyzed by immunoblotting with anti-Beclin 1 antibody to detect ubiquitylated Beclin 1. The ubiquitination of Beclin 1 by cIAP1 was reduced upon overexpression of TRADD, which was restored by Apt-1. For gel source data, see Supplementary Figure 1.

Extended Data Figure 7. ICCB-19/Apt-1 inhibit inflammatory responses. a, MEFs were stimulated by mTNFα (10 ng/ml) in the presence of vehicle or ICCB-19 (10 μM) for indicated time. NF-κB and MAPKs activity were determined by immunoblotting using indicated abs. **b**, MEFs were stimulated by mTNFα (10 ng/ml) in the presence of vehicle or ICCB-19 (10 μM) for indicated time. The protein levels of iNOS and Cox2 were determined by immunoblotting. **c**-**g**,

BV2 cells (a microglial-like cell line) (**c**, **d**, **e**) and BMDMs (bone marrow-derived macrophages) (**f**, **g**) were treated with IFNγ (**c**, 1 unit/μl), Pam3CSK4 (ligand for TLR2) (**e**, 10 ng/ml), LPS (ligand for TLR4) (**f**, 10 ng/ml), or MDP (ligand for NOD2/RIPK2 pathway) (**d**, **g**, 10 μg/ml) for indicated time. The mRNA levels of TNFα were determined using quantitative PCR. Mean ± s.d. of $n = 3$ biologically independent samples, representative of 3 independent experiments (**c**-**g**). **h**, BV2 cells were treated with IFNγ (1 unit/μl) together with Apt-1 (10 μM) or Nec-1s (10 μM) for 24 h. TNFα production was determined by ELISA. **i**, BV2 cells were pretreated with Apt-1 (10 μM) or Nec-1s (10 μM) for 1 h and then MDP (10 μg/ml) was added to cells together with transfection reagent for 7 h. TNFα production was determined by ELISA. **j**, BV2 cells were pretreated with Apt-1 (10 μM) or Nec-1s (10 μM) and then treated with Pam3CSK4 (10 ng/ml) for 8 h. TNFα production was determined by ELISA. **k**, BMDMs were pretreated with Apt-1 (10 μM) or Nec-1s (10 μM) for 1h and then treated with LPS (10 ng/ml) for 7 h. TNFα production was determined by ELISA. **l**, BMDMs were first primed with IFNγ (10 ng/ml) for 2 h and then removed. The cells were then treated with Apt-1 (10 μM) or Nec-1s (10 μM) for 1 h and MDP (10 μg/ml) was added to cells directly and treated for 8 h. TNFα production was determined by ELISA. Mean ± s.d. of $n = 3$ biologically independent samples, representative of 3 independent experiments (**h**-**l**). **m**, BMDMs were treated with LPS (10 ng/ml) in the presence of vehicle control or Apt-1 (10 μM) or Nec-1s (10 μM) for indicated time. NF-κB and MAPKs activity were determined by immunoblotting using indicated abs. **n**, Body temperature was measured in male mice ($n = 10$, 8 weeks) injected with mTNFα (9.5 μg, i.v.) after pretreatment with Apt-1 (20 mg/kg) 30 min before. Control mice ($n = 9$) received an equal amount of vehicle before mTNFα challenge. Mean ± s.e.m. Two-way ANOVA. $^{***}P = 0.0007$. **o**, Kaplan Meier Survival Curve was measured on mice treated as in (**n**). Two-sided log-rank (Mantel-Cox) test. $^{***}P = 1 \times 10^{-5}$. For gel source data, see Supplementary Figure 1.

Extended Data Figure 8. Restoring proteome homeostasis by ICCB-19/Apt-1. a, **b**, Parallel wells of PC12/Htt-Q103 cells were cultured with Vehicle, ICCB-19 (10 μM), ICCB-19i (10 μM), Apt-1 (10 μM), Nec-1s (10 μM), and zVAD (20 μM) as indicated prior to the addition of Ponasterone A (5 μM) for 48 h. Nuclei were labeled with DAPI. The amount of Htt-Q103-EGFP aggregates per mm^2 was quantified using ImageJ. Cell viability was measured by CellTiter-Glo assay. Survival rate is compared with vehicle-treated cells (**b**). Mean ± s.d. of $n = 3$ (**a**), $n = 4$ (**b**) biologically independent samples, representative of 3 independent experiments. One-way ANOVA, post hoc Dunnett's tests. $^{***}P = 1 \times 10^{-5}$ (left to right, **a**, **b**); n.s. not significant, (P = 0.8556, 0.9195, 0.8613, 0.5687, 0.5304, 0.9998, 0.6029, 0.2821 (left to right, **a**, **b**)). **c**, **d**, SH-SY5Y cells were transfected with expression vectors for RFP-α-Synuclein WT, E46K, or A53T for 24h and then treated with vehicle or Apt-1 (10 μM) for 24 h. RFP-α-Synuclein was quantified by Fluorescence/Cell (RLU) by ImageJ. The cells treated as in (**c**) were lysed and analyzed by immunoblotting for the levels of α-Synuclein (**d**). Mean ± s.d. of $n = 3$ biologically independent samples, representative of 3 independent experiments. Two-way ANOVA, post hoc Bonferroni's tests. $^{***}P = 8 \times 10^{-5}$; $^{*}P$ = 0.0262, 0.0367 (left to right, **c**). **e**, **f**, Quantification of GFP-Tau fluorescence (**e**) or immunoblots of tau levels (**f**) in H4 cells treated with Apt-1. Mean ± s.d. of $n = 3$ biologically independent samples, representative of 3 independent experiments. Two-way ANOVA, post hoc Bonferroni's tests. $^{***}P = 8 \times 10^{-5}$, 8×10^{-4} (**e**, left to right). **g**, Representative images and quantification of cultured brain slices from PS19 mice (4 months old) stained with phospho-tau (red) and cell nuclei (DAPI/blue). Mean ± s.e.m. of $n = 5$ biologically independent samples. Two-tailed t-test. **h**, Immunoblots of tau levels in cultured PS19 mouse (4 months old) brain slices treated with indicated compounds. **i**, Pharmacokinetics of Apt-1 over 24 h dosing period in cerebrospinal fluid (CSF) and hippocampus. Apt-1 was delivered using

intracerebroventricular Alzet micro-osmotic pump (20 mM Apt-1, 100 µl, release rate: 0.25 µl/h). CSF was collected at 1 h, 6 h, and 24 h. Hippocampi were collected at 24 h. The concentrations of Apt-1 were measured by HPLC. The concentration of Apt-1 in hippocampus at 24 h was 6.27 µM. Mean ± s.e.m. (n = 3 mice in each group). **j**, **k**, Synthetic preformed fibrils (pffs) [5µg full length tau (2N4R) with P301S mutation (T40/PS) per injection] or vehicle were injected into the hippocampi of PS19 mice (8 weeks old). Three weeks after the pffs injection, Apt-1 was delivered intracerebroventrically by Alzet micro-osmotic pumps (20 mM Apt-1, release rate 0.25µl/h) for one week before sacrificing. The hippocampi were isolated from the mice for immunoblotting using TAU-5 (Thermo Fisher) (**j**), or immunostaining for phospho-Tau (AT8) (**k**). Dots represent the mean from individual mice. Mean ± s.e.m. (n = 3 mice in each group). Two-tailed t-test. $^{***}P$ = 0.0007. For gel source data, see Supplementary Figure 1.

Extended Data Figure 9. ICCB-19/Apt-1 reduce the interaction of TRADD and TRAF2. a, Expression constructs encoding Flag-TRADD-N (1-179) and HA-TRADD-C (180-312) were transfected into HEK293T cells for 18 h. Then the cells were treated with Apt-1 (10 µM) or vehicle for another 6 h. The binding between Flag-TRADD-N (1-179) and HA-TRADD-C (180-312) was analyzed by Co-IP assay as indicated. **b-d**, The effect of Apt-1 and ICCB-19 on the binding between TRADD-N and TRADD-C was determined by NanoBiT assay. Constructs were made encoding LgBiT and SmBiT fused to the N and C termini of TRADD-N and TRADD-C, respectively. HEK293T cells were transfected with these two plasmids for 24 h and then treated with indicated compounds for 6 h. The luminescence indicating the interaction of TRADD-N and TRADD-C was measured using Nano-Glo Live Cell Reagent. **e**, Test of the Nano-Bit system assay using a known binding pair: PRKAR2A and PRKACA. **f**, Apt-1 (10 µM) does not affect the Nano-Bit system assay as determined by using the known binding pair: PRKAR2A and PRKACA. **g**,

Apt-1 reduces the binding between TRADD-N and TRAF2-C in a dose-dependent manner as determined by NanoBiT assay. **h**, Schematic representation of a cell-free Förster resonance energy transfer (FRET)-based assay to detect TRADDN and TRAF2C interaction. **i**, Purification of indicated proteins for FRET assay expressed in HEK293T cells. Proteins were pulled down by anti-Flag affinity gel and eluted by 3×Flag peptide. CBB staining of the proteins are shown on the right. **j**, FRET-based assay to measure the direct interaction of TRADD-N and TRAF2-C was developed in which the donor Flag-TRAF2C-mCenulean (TRAF2C-mC) was excited at 430 nm, and the emission was measured from 450 to 600 nm. When FRET occurs, the acceptor mVenus-TRADDN-Flag (mV-TRADDN) emission will increase and the donor emission will decrease. Apt-1 was added to the system with indicated concentration and incubated for 1h, then subjected to FRET assay. **k**, Effect of TRAF2 on the binding between TRADD-N and TRADD-C was determined by NanoBiT assay. HEK293T cells were transfected with the plasmids as indicated for 24h and then treated with Apt-1 (10μM) for 4h, then luminescence was measured. **l**, U937 cells were stimulated with TNFα (10 ng/ml) for indicated minutes in the presence of vehicle or Apt-1 (10 μM) and the complex I was pulled down using anti-TNFR1. Levels of cIAP1, TRAF2, and TRADD recruitment were determined by immunoblotting. Quantifications of cIAP1, TRAF2, and TRADD are shown below each blot. **m**, Due to the lack of a good anti-TRADD antibody for immunoprecipitation, *Tradd*$^{-/-}$ MEFs were reconstituted with Flag-mTRADD. Cells were treated with indicated concentrations of Apt-1 for 12 h, then co-IP was performed using anti-Flag antibody followed by immunoblotting using indicated antibodies. Mean ± s.d. of $n = 3$ (**e**, **f**), $n = 4$ (**c**, **g**), $n = 5$ (**b**), $n = 6$ (**d**, **k**) biologically independent samples, representative of 3 independent experiments. One-way ANOVA, post hoc Dunnett's test. $^{***}P = 1 \times 10^{-15}$ (**b**, left to right), $^{***}P = 1 \times 10^{-15}$, n.s. not significant, ($P = 0.3357$) (**d**). $^{***}P = 1 \times 10^{-15}$ (**k**, left to right). For gel source data, see Supplementary Figure 1.

Extended Data Figure 10. ICCB-19/Apt-1 bind to TRADD-N. A fluorescence-based thermal shift assay was developed to quantify ICCB-19/Apt-1 binding to TRADD by measuring changes in thermal denaturation temperature (Tm). **a**, CBB staining of GST-tag and GST-TRADD purified from HEK293T cells. **b**, *in vitro* binding of GST-TRADD (50 μM) with ICCB-19 (250 μM) and Apt-1 (250 μM) was determined by thermal shift assay. Thermal unfolding of GST-TRADD is monitored using SYPRO Orange. Data were collected in the presence of ICCB-19 and Apt-1, leading to a rightward shift in the unfolding transition. The apparent melting temperature (Tm) is the peak in the derivative of the unfolding curve (dF/dT), which is used as an indicator of thermal stability. **c**, GST-tag (50 μM) does not bind to the compounds (250 μM) as determined by thermal shift assay. **d**, ICCB-19i does not bind to GST-TRADD as determined by thermal shift assay. **e**, GST-TRADD-C (50 μM) alone does not bind to either ICCB-19 (250 μM) or Apt-1 (250 μM) as determined by thermal shift assay. **f-h**, TRADD-N/ICCB-19 (**f**), TRADD-N/Apt-1 (**g**), and TRADD-N/ICCB-19i (**h**) samples used for STD NMR experiments were prepared as 1 mM ICCB-19 (**f**), 1 mM Apt-1 (**g**), 1 mM ICCB-19i (**h**), and 13 μM TRADD-N in 0.5 mL of PBS in D_2O (10%). The on-resonance irradiation of TRADD-N was performed at a chemical shift of -0.5 ppm, whereas the off-resonance irradiation was conducted at 37 ppm. Spectra were acquired using the following parameters: spectral window of 6.4 kHz, number of scans at 320, acquisition time of 2 s, and repetition time of 3 s. The decrease in signal intensity in STD spectrum, resulting from the transfer of saturation from the protein to the ligand, is evaluated by subtracting the on-resonance spectrum from the off-resonance spectrum. This subtraction yields a positive signal from a bound ligand. The asterisks indicate the signals of the compounds. The STD data suggest that both ICCB-19/Apt-1, but not ICCB-19i, bind with TRADD-N. **i**, CBB staining of 6×His- and Flag-tagged TRADD for SPR purified from HEK293T cells. The proteins were pulled down by anti-Flag

affinity gel and eluted by 3×Flag peptide. The proteins were further purified by size exclusion chromatograph on a Superdex 75 column (GE Healthcare) in a buffer containing 20 mM imidazole (pH 6.6), 200 mM NaCl, 20 mM DTT. **j**, BIAcore SPR analysis of ICCB-19 binding to TRADD-N. The kinetic profile of ICCB-19 binding to TRADD-N is shown. A series of concentrations of ICCB-19 (ranging from 0.3125 to 10 μM) was used to measure the binding kinetics, with TRADD-N immobilized on the CM5 chip.

Extended Data Figure 11. The binding mechanism of ICCB-19/Apt-1 on TRADD. a-c, Superposition of 2D ^{1}H-^{15}N HSQC spectra of ^{15}N-labeled His-TRADD-N (250 μM) in the presence (red) and absence (blue) of Apt-1 (500 μM) (**a**), ICCB-19 (500 μM) (**b**) or ICCB-19i (500 μM) (**c**). The close-up view of the region exhibited large perturbations was shown right. **d**, Binding pose of ICCB-19 in complex with TRADD-N was generated by induced-fit docking. The left panel demonstrated the shape and polarity of the ligand binding pocket surface, with red regions indicating negatively charged and blue positively charged. The right panel showed details of the interactions between the compound and TRADD-N. The compound was shown as cyan sticks, and the protein was shown as pink cartoon with key residues highlighted in sticks. Hydrogen bonds were shown as red dashed lines. **e**, Coomassie blue staining of WT and each mutant protein for thermal shift assay. **f**, **g,** HEK293T cells were seeded at 7.5×10^{3} cells per well in a white, clear-bottom 96-well plate 24 h before transfection. Cells were then transfected with the indicated plasmids for 24h. Medium was removed and replaced with Opti-MEM medium (100 μl) for 1 h at 37 °C. The Nano-Glo reagent was prepared and added to each well immediately before the luminescence reading was taken. Luminescence was measured immediately on a plate reader and reported as relative light units (RLU). Mean ± s.d. of n = 6 biologically independent samples, representative of 3 independent experiments.

Extended Data Figure 12. A mutagenesis study of ICCB-19/Apt-1 binding with TRADD to inhibit RDA and activate autophagy. a, *Tradd*$^{-/-}$ MEFs were reconstituted with Flag-tagged WT or mutant TRADD as indicated. Expression levels of TRADD were determined by immunoblotting. **b**, *Tradd*$^{-/-}$ MEFs transfected with Flag-tagged WT or indicated TRADD mutants were stimulated by TNFα/5z7 for 9 h in the presence or absence of Apt-1 (10 μM). Cell survival was determined by CellTiter-Glo assay. Mean ± s.d. of $n = 3$ biologically independent samples, representative of 3 independent experiments. Two-tailed t-test. **c**, **d**, TRADD-N(G121A)/Apt-1 (**c**), and TRADD-N(G121A)/ICCB-19 (**d**) samples for STD-NMR analyses were prepared as that of WT TRADD in (**10f**) with 1 mM Apt-1 (**c**), 1 mM ICCB-19 (**d**), and 13 μM TRADD-N(G121A) in 0.5 mL of PBS in D_2O (10%). **e**, BIAcore SPR analysis of Apt-1 binding to TRADD-N(G121A). The kinetic profile of Apt-1 binding to TRADD-N(G121A) is shown. A series of concentrations of Apt-1 (ranging from 0.15625 to 5 μM) was used to measure the binding kinetics, with TRADD-N(G121A) immobilized on the CM5 chip. **f**, *Tradd*$^{-/-}$ MEFs were reconstituted with Flag-tagged WT or indicated TRADD mutants. The expression levels of TRADD were determined by immunoblotting. **g**, **h**, *Tradd*$^{-/-}$ MEFs reconstituted with Flag-mutant TRADD (Y16A/F18A or Y16A/I72A/R119A) were stimulated by TNFα/5z7 for indicated time in the presence or absence of Apt-1 (10 μM). The cell survival was determined by CellTiter-Glo assay. Mean ± s.d. of $n = 3$ biologically independent samples, representative of 3 independent experiments. **i**, A model for mechanism by which Apt-1 targets TRADD to inhibit RDA and activate autophagy. In TNFα-stimulated cells: Apt-1 binds to TRADD-N to reduce its binding with TRADD-C which stabilizes the binding of TRADD mediated by its DD in TRADD-C with the DD in TNFR1. The binding of Apt-1 with TRADD in complex I modulates the K63/M1 ubiquitination of RIPK1 by reducing the binding of TRADD with TRAF2/cIAP1/2 which increases the recruitment of A20 and HOIP to inhibit the activation of

RIPK1 kinase. Increased retention of TRADD in complex I also decreases cytosolic availability of TRADD for the formation of complex IIa in which TRADD is known to be a key component. Treatment with Apt-1 also reduces the activation of NF-κB in TNFα-stimulated cells. In autophagy pathway: TRADD normally binds to TRAF2 and cIAP1/2 homeostatically. Apt-1 can release TRAF2 and cIAP1/2 from their binding with TRADD. Released TRAF2/cIAP1/2 in turn mediates K63 ubiquitination of Beclin 1 to promote the formation of Vps34 complex, production of PtdIns3P, and activation of autophagy. For gel source data, see Supplementary Figure 1.

Fig. 1

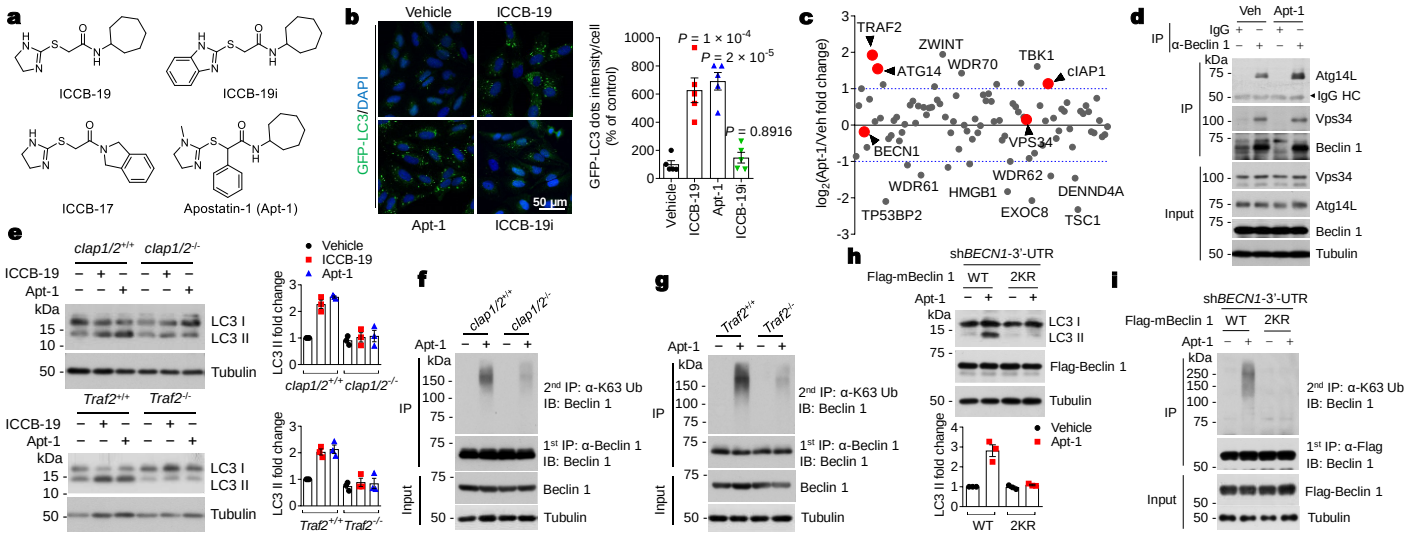
a
ICCB-19
ICCB-19i
ICCB-17
Apostatin-1 (Apt-1)
b
Vehicle
ICCB-19
GFP-LC3/DAPI
50 μm
Apt-1
ICCB-19i
GFP-LC3 dots intensity/cell (% of control)
P = 1 × 10-4
P = 2 × 10-5
P = 0.8916
Vehicle
ICCB-19
Apt-1
ICCB-19i
c
log2(Apt-1/Veh fold change)
TRAF2
ZWINT
ATG14
WDR70
TBK1
cIAP1
BECN1
VPS34
WDR62
WDR61
HMGB1
DENND4A
EXOC8
TP53BP2
TSC1
d
Veh
Apt-1
IP
IgG
α-Beclin 1
kDa
Atg14L
IgG HC
Vps34
Beclin 1
Input
Tubulin
e
clap1/2+/+
clap1/2-/-
ICCB-19
Apt-1
kDa
LC3 I
LC3 II
Tubulin
Vehicle
ICCB-19
Apt-1
LC3 II fold change
Traf2+/+
Traf2-/-
f
clap1/2+/+
clap1/2-/-
Apt-1
IP
Input
2nd IP: α-K63 Ub
IB: Beclin 1
1st IP: α-Beclin 1
IB: Beclin 1
Beclin 1
Tubulin
g
Traf2+/+
Traf2-/-
h
shBECN1-3'-UTR
Flag-mBeclin 1
WT
2KR
Flag-Beclin 1
i
shBECN1-3'-UTR
Flag-mBeclin 1
WT
2KR
1st IP: α-Flag
IB: Beclin 1
Flag-Beclin 1

Fig. 2

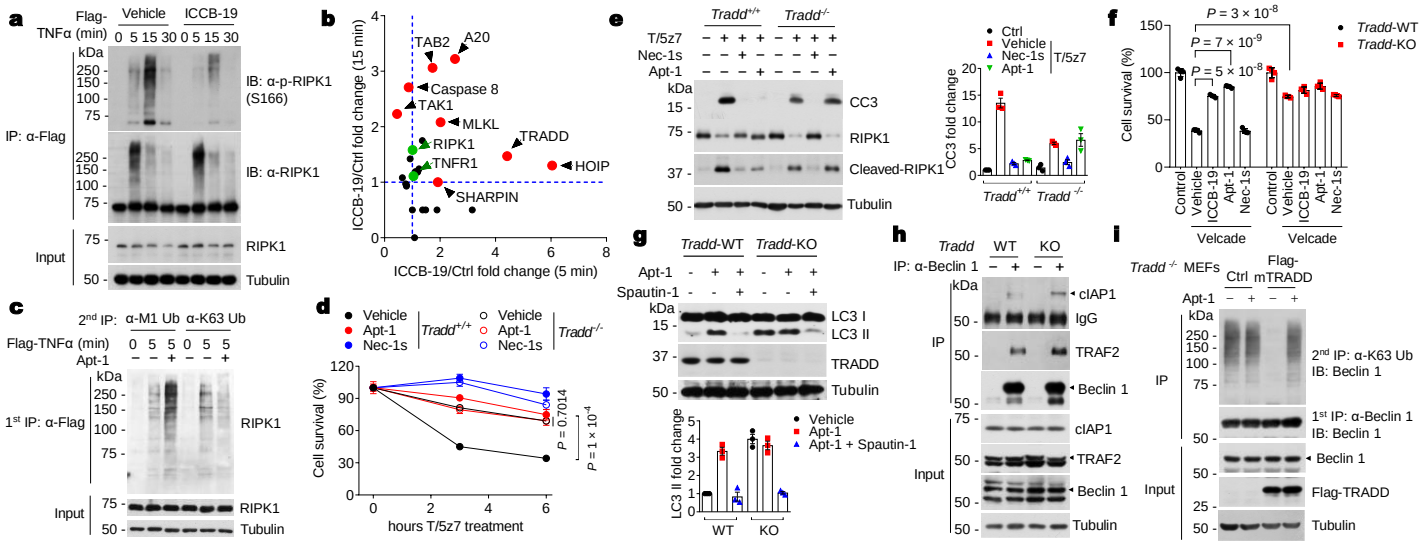
a
Flag-TNFα (min)
Vehicle
ICCB-19
0 5 15 30 0 5 15 30
kDa
250
150
100
75
IP: α-Flag
IB: α-p-RIPK1 (S166)
IB: α-RIPK1
Input
RIPK1
Tubulin
50
b
ICCB-19/Ctrl fold change (15 min)
ICCB-19/Ctrl fold change (5 min)
TAB2
A20
Caspase 8
TAK1
MLKL
RIPK1
TRADD
TNFR1
HOIP
SHARPIN
c
2nd IP: α-M1 Ub α-K63 Ub
Flag-TNFα (min)
Apt-1
1st IP: α-Flag
RIPK1
Input
Tubulin
d
Vehicle
Apt-1
Nec-1s
Tradd+/+
Tradd-/-
Cell survival (%)
hours T/5z7 treatment
P = 0.7014
P = 1 × 10-4
e
Tradd+/+
Tradd-/-
T/5z7
Nec-1s
Apt-1
kDa
CC3
RIPK1
Cleaved-RIPK1
Tubulin
Ctrl
Vehicle
Nec-1s
Apt-1
T/5z7
CC3 fold change
f
P = 3 × 10-8
P = 7 × 10-9
P = 5 × 10-8
Tradd-WT
Tradd-KO
Cell survival (%)
Control
Vehicle
ICCB-19
Apt-1
Nec-1s
Velcade
g
Tradd-WT
Tradd-KO
Apt-1
Spautin-1
kDa
LC3 I
LC3 II
TRADD
Tubulin
LC3 II fold change
Vehicle
Apt-1
Apt-1 + Spautin-1
WT
KO
h
Tradd
WT
KO
IP: α-Beclin 1
cIAP1
IgG
TRAF2
Beclin 1
Input
i
Tradd-/- MEFs
Ctrl
Flag-mTRADD
Apt-1
2nd IP: α-K63 Ub
IB: Beclin 1
1st IP: α-Beclin 1
Flag-TRADD

Fig. 3

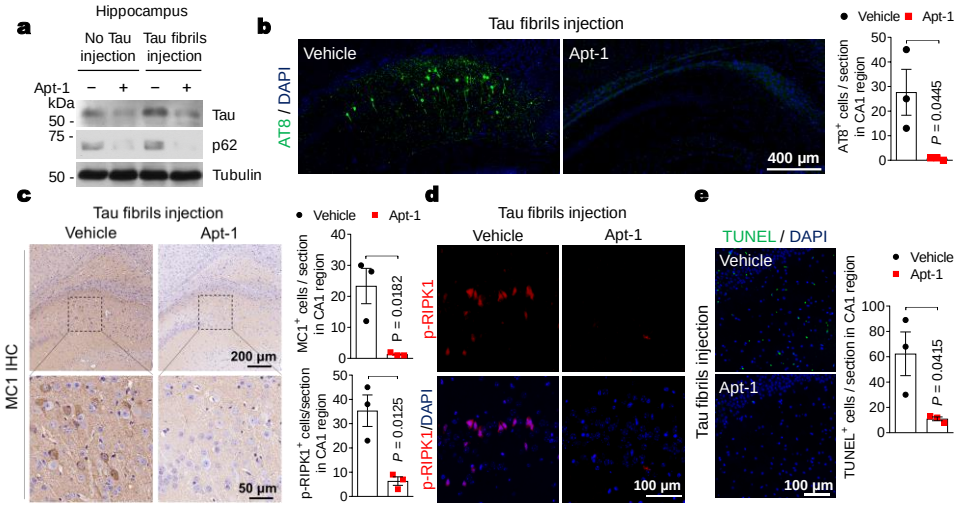
a
Hippocampus
No Tau injection
Tau fibrils injection
Apt-1 – + – +
kDa
50 -
75 -
Tau
p62
50 -
Tubulin
b
Tau fibrils injection
Vehicle
Apt-1
AT8 / DAPI
400 μm
Vehicle
Apt-1
AT8+ cells / section in CA1 region
P = 0.0445
c
Tau fibrils injection
Vehicle
Apt-1
MC1 IHC
200 μm
50 μm
Vehicle
Apt-1
MC1+ cells / section in CA1 region
P = 0.0182
p-RIPK1+ cells/section in CA1 region
P = 0.0125
d
Tau fibrils injection
Vehicle
Apt-1
p-RIPK1
p-RIPK1/DAPI
100 μm
e
TUNEL / DAPI
Vehicle
Apt-1
Tau fibrils injection
100 μm
Vehicle
Apt-1
TUNEL+ cells / section in CA1 region
P = 0.0415

Fig. 4

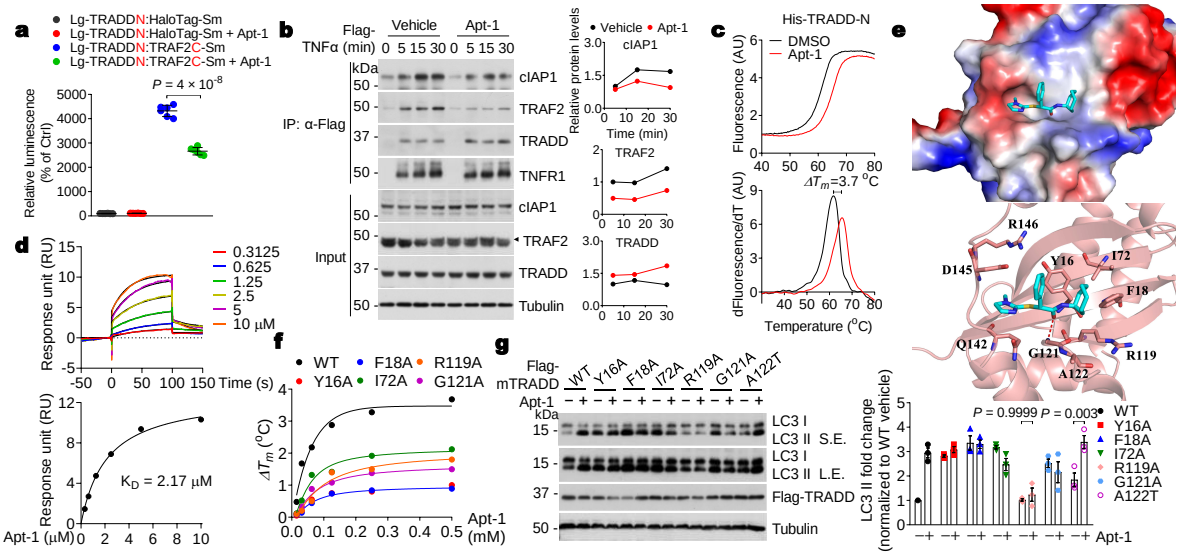
a
Lg-TRADDN:HaloTag-Sm
Lg-TRADDN:HaloTag-Sm + Apt-1
Lg-TRADDN:TRAF2C-Sm
Lg-TRADDN:TRAF2C-Sm + Apt-1
P = 4 × 10-8
Relative luminescence (% of Ctrl)
b
Flag-
Vehicle
Apt-1
TNFα (min) 0 5 15 30 0 5 15 30
kDa
cIAP1
TRAF2
TRADD
TNFR1
IP: α-Flag
Input
Tubulin
Relative protein levels
Vehicle Apt-1
Time (min)
c
His-TRADD-N
DMSO
Apt-1
Fluorescence (AU)
ΔTm=3.7 °C
dFluorescence/dT (AU)
Temperature (°C)
d
Response unit (RU)
0.3125
0.625
1.25
2.5
5
10 μM
Time (s)
KD = 2.17 μM
Apt-1 (μM)
e
R146
D145
Y16
I72
F18
Q142
G121
R119
A122
f
WT
F18A
R119A
Y16A
I72A
G121A
ΔTm (°C)
Apt-1 (mM)
g
Flag-mTRADD
WT
Y16A
F18A
I72A
R119A
G121A
A122T
Apt-1
LC3 I
LC3 II S.E.
LC3 I
LC3 II L.E.
Flag-TRADD
Tubulin
LC3 II fold change (normalized to WT vehicle)
P = 0.9999
P = 0.003
WT
Y16A
F18A
I72A
R119A
G121A
A122T
Apt-1

Extended Data Figure 1

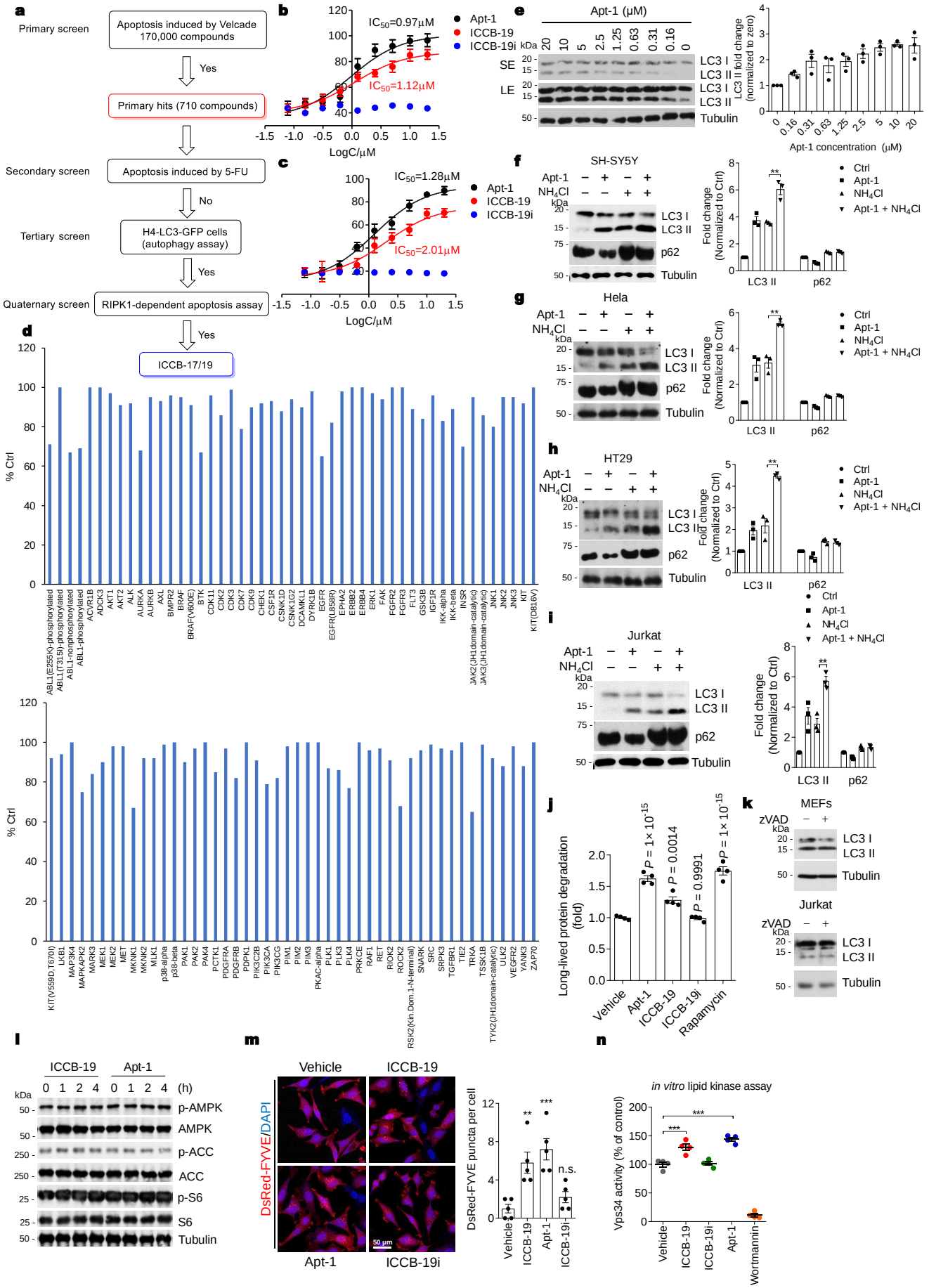

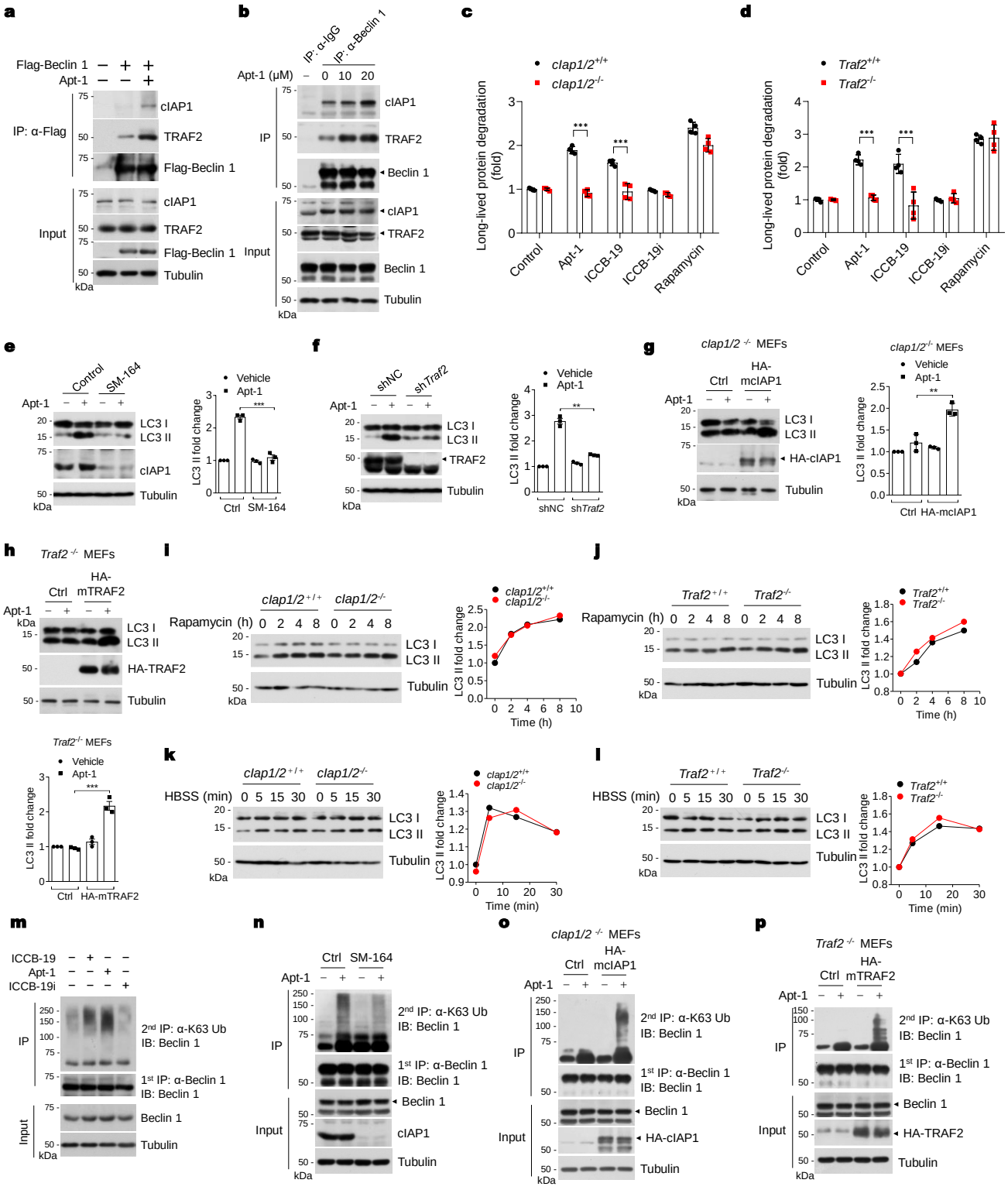
a
Flag-Beclin 1
Apt-1
IP: α-Flag
cIAP1
TRAF2
Flag-Beclin 1
Input
Tubulin
kDa
b
IP: α-IgG
IP: α-Beclin 1
Apt-1 (μM)
Beclin 1
c
clap1/2+/+
clap1/2-/-
Long-lived protein degradation (fold)
Control
Apt-1
ICCB-19
ICCB-19i
Rapamycin
d
Traf2+/+
Traf2-/-
e
Control
SM-164
LC3 I
LC3 II
LC3 II fold change
Vehicle
Ctrl
f
shNC
shTraf2
TRAF2
shNC
shTraf2
g
clap1/2 -/- MEFs
HA-mcIAP1
HA-cIAP1
h
Traf2 -/- MEFs
HA-mTRAF2
i
Rapamycin (h)
Time (h)
j
k
HBSS (min)
Time (min)
l
m
ICCB-19
ICCB-19i
2nd IP: α-K63 Ub
IB: Beclin 1
1st IP: α-Beclin 1
n
o
p

a

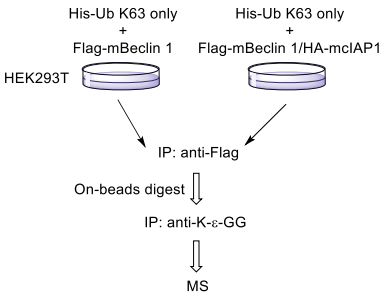

b

HEK293T_IP_Flag-mBeclin 1_GlyGly(K) sites			
Positions within proteins	**Intensity mBeclin1**	**Intensity mBeclin1 mcIAP1**	**Ratio**
183	263950000	451099000	1.709032014
204	113540000	183964000	1.620257178
201	24357000	31848300	1.307562508
398	52814000	63685600	1.205846935
235	89136000	93790400	1.052216837
322	40192000	40766000	1.014281449
263	64402000	59782800	0.928275519
246	2808300	2479290	0.882843713
261	89979000	77105600	0.856928839

c

```
Mus musculus          181_ELKELALEEERLIQELEDVEKNRKVVA_207
Homo sapiens          183_ELKELALEEERLIQELEDVEKNRKIVA_209
Rattus norvegicus     181_ELKELALEEERLIQELEDVEKNRKVVA_207
Bos Taurus            181_ELKELALEEERLIQELEDVEKNRKIVA_207
Felis catus           181_ELKELALEEERLIQELEDVEKNRKIVA_207
Gallus gallus         180_ELKELALEEEQLIQELEDVEKNRKIVA_206
Myotis lucifugus      181_ELKELALEEERLIQELEDVEKNRKLVA_207
```

d

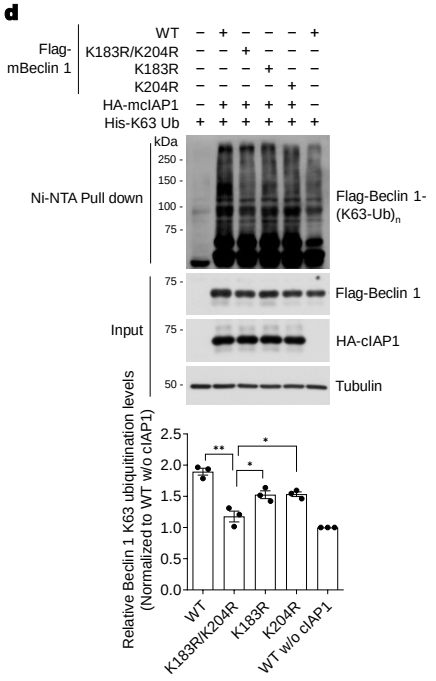

e

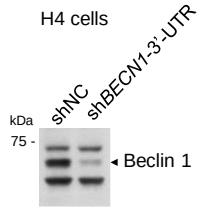

f

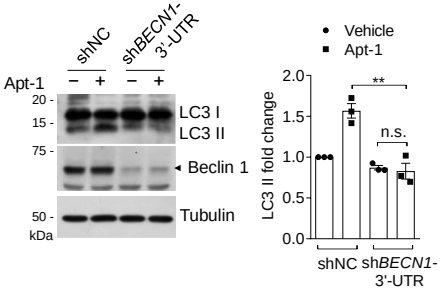

g

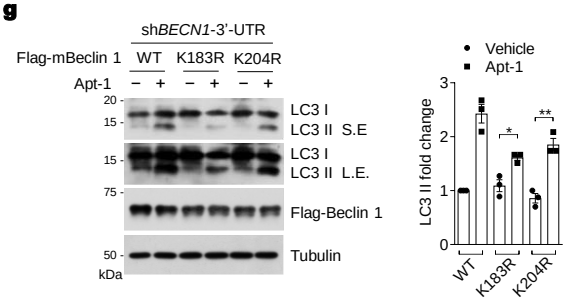

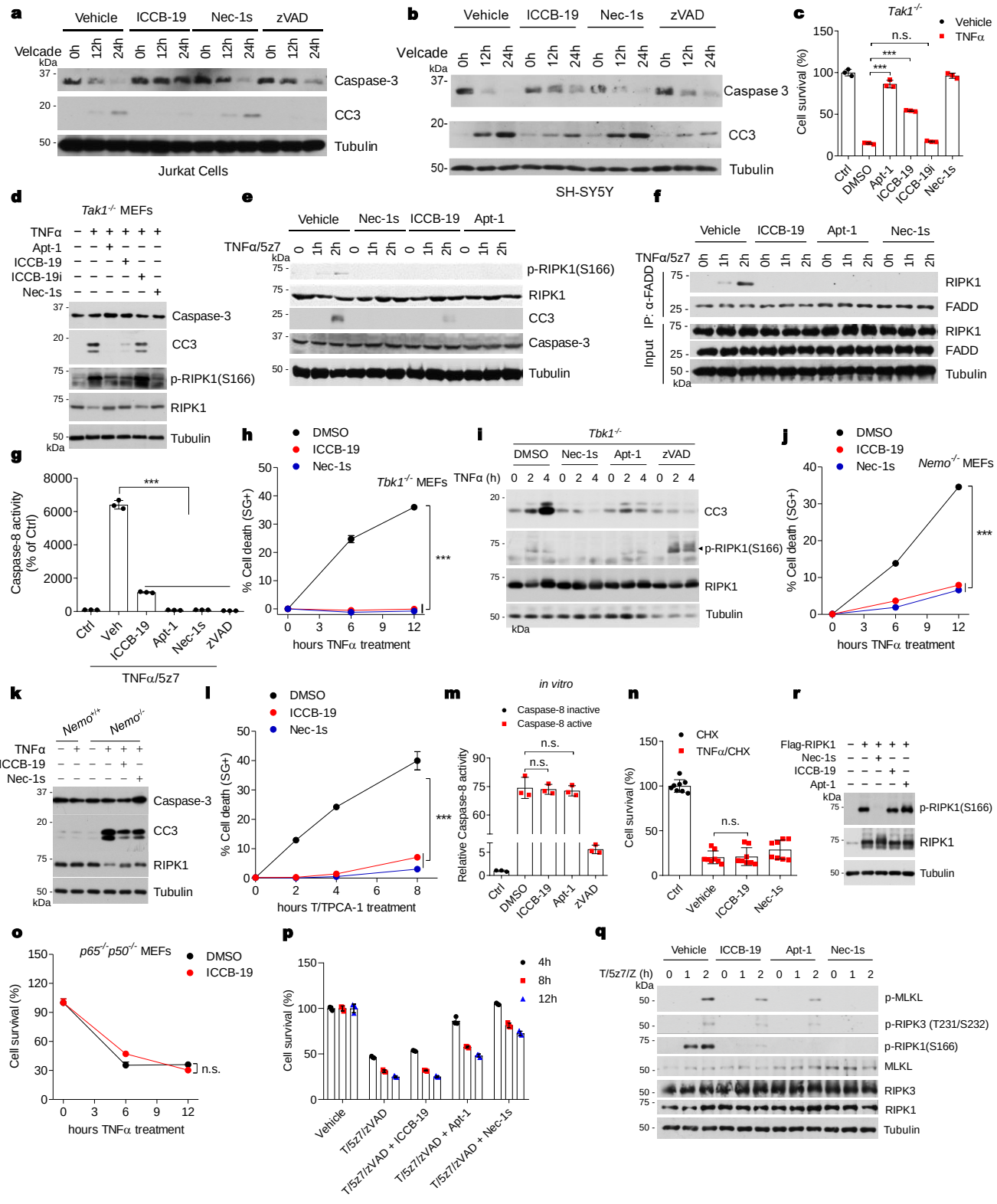
a
Vehicle
ICCB-19
Nec-1s
zVAD
Velcade
0h 12h 24h 0h 12h 24h 0h 12h 24h 0h 12h 24h
kDa
37 -
20 -
50 -
Caspase-3
CC3
Tubulin
Jurkat Cells
b
Vehicle
ICCB-19
Nec-1s
zVAD
Velcade
0h 12h 24h 0h 12h 24h 0h 12h 24h 0h 12h 24h
kDa
37-
20-
50-
Caspase 3
CC3
Tubulin
SH-SY5Y
c
Tak1-/-
Vehicle
TNFα
Cell survival (%)
150
100
50
0
n.s.
***
***
Ctrl
DMSO
Apt-1
ICCB-19
ICCB-19i
Nec-1s
d
Tak1-/- MEFs
TNFα
Apt-1
ICCB-19
ICCB-19i
Nec-1s
Caspase-3
CC3
p-RIPK1(S166)
RIPK1
Tubulin
kDa
e
Vehicle
Nec-1s
ICCB-19
Apt-1
TNFα/5z7
0 1h 2h 0 1h 2h 0 1h 2h 0 1h 2h
kDa
p-RIPK1(S166)
RIPK1
CC3
Caspase-3
Tubulin
f
Vehicle
ICCB-19
Apt-1
Nec-1s
TNFα/5z7
0h 1h 2h 0h 1h 2h 0h 1h 2h 0h 1h 2h
IP: α-FADD
Input
RIPK1
FADD
RIPK1
FADD
Tubulin
kDa
g
Caspase-8 activity (% of Ctrl)
8000
6000
4000
2000
0
***
Ctrl
Veh
ICCB-19
Apt-1
Nec-1s
zVAD
TNFα/5z7
h
DMSO
ICCB-19
Nec-1s
Tbk1-/- MEFs
% Cell death (SG+)
50
40
30
20
10
0
***
0 3 6 9 12
hours TNFα treatment
i
Tbk1-/-
DMSO
Nec-1s
Apt-1
zVAD
TNFα (h)
0 2 4 0 2 4 0 2 4 0 2 4
CC3
p-RIPK1(S166)
RIPK1
Tubulin
kDa
j
DMSO
ICCB-19
Nec-1s
Nemo-/- MEFs
% Cell death (SG+)
40
30
20
10
0
***
0 3 6 9 12
hours TNFα treatment
k
Nemo+/+
Nemo-/-
TNFα
ICCB-19
Nec-1s
Caspase-3
CC3
RIPK1
Tubulin
kDa
l
DMSO
ICCB-19
Nec-1s
% Cell death (SG+)
50
40
30
20
10
0
***
0 2 4 6 8
hours T/TPCA-1 treatment
m
in vitro
Caspase-8 inactive
Caspase-8 active
Relative Caspase-8 activity
90
75
60
5
0
n.s.
n.s.
Ctrl
DMSO
ICCB-19
Apt-1
zVAD
n
CHX
TNFα/CHX
Cell survival (%)
150
100
50
0
n.s.
Ctrl
Vehicle
ICCB-19
Nec-1s
r
Flag-RIPK1
Nec-1s
ICCB-19
Apt-1
kDa
p-RIPK1(S166)
RIPK1
Tubulin
o
p65-/-p50-/- MEFs
DMSO
ICCB-19
Cell survival (%)
150
120
90
60
30
0
n.s.
0 3 6 9 12
hours TNFα treatment
p
4h
8h
12h
Cell survival (%)
150
100
50
0
Vehicle
T/5z7/zVAD
T/5z7/zVAD + ICCB-19
T/5z7/zVAD + Apt-1
T/5z7/zVAD + Nec-1s
q
Vehicle
ICCB-19
Apt-1
Nec-1s
T/5z7/Z (h)
0 1 2 0 1 2 0 1 2 0 1 2
kDa
p-MLKL
p-RIPK3 (T231/S232)
p-RIPK1(S166)
MLKL
RIPK3
RIPK1
Tubulin

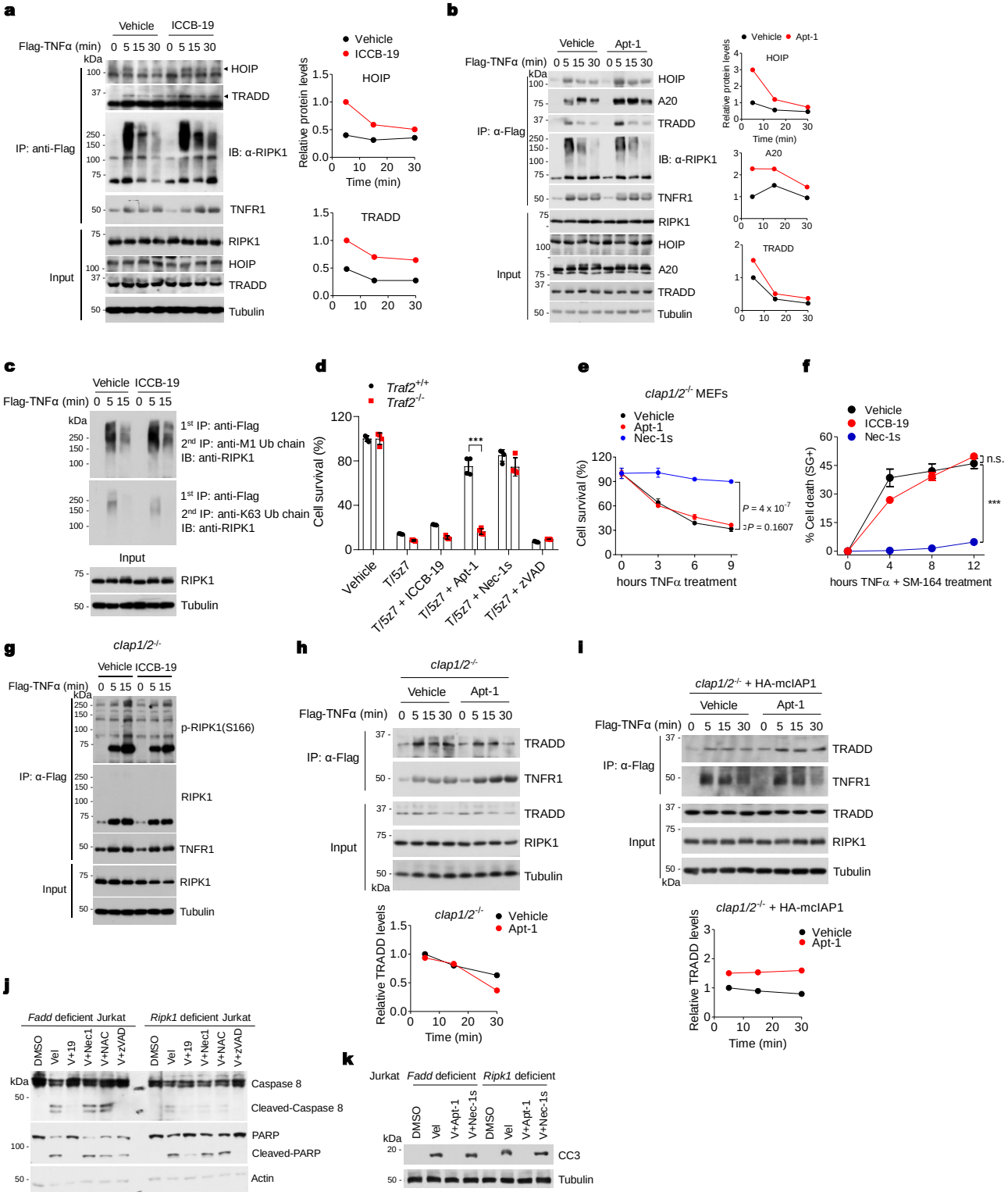
a
Vehicle
ICCB-19
Flag-TNFα (min) 0 5 15 30 0 5 15 30
kDa
HOIP
TRADD
IP: anti-Flag
IB: α-RIPK1
TNFR1
RIPK1
Input
HOIP
TRADD
Tubulin
Relative protein levels
Time (min)
b
Vehicle
Apt-1
Flag-TNFα (min) 0 5 15 30 0 5 15 30
HOIP
A20
TRADD
IP: α-Flag
IB: α-RIPK1
TNFR1
RIPK1
Input
HOIP
A20
TRADD
Tubulin
c
Vehicle ICCB-19
Flag-TNFα (min) 0 5 15 0 5 15
1st IP: anti-Flag
2nd IP: anti-M1 Ub chain
IB: anti-RIPK1
1st IP: anti-Flag
2nd IP: anti-K63 Ub chain
IB: anti-RIPK1
Input
RIPK1
Tubulin
d
Traf2+/+
Traf2-/-
Cell survival (%)
***
Vehicle
T/5z7
T/5z7 + ICCB-19
T/5z7 + Apt-1
T/5z7 + Nec-1s
T/5z7 + zVAD
e
clap1/2-/- MEFs
Vehicle
Apt-1
Nec-1s
Cell survival (%)
P = 4 x 10-7
P = 0.1607
hours TNFα treatment
f
Vehicle
ICCB-19
Nec-1s
% Cell death (SG+)
n.s.
***
hours TNFα + SM-164 treatment
g
clap1/2-/-
Vehicle ICCB-19
Flag-TNFα (min) 0 5 15 0 5 15
kDa
p-RIPK1(S166)
IP: α-Flag
RIPK1
TNFR1
Input
RIPK1
Tubulin
h
clap1/2-/-
Vehicle
Apt-1
Flag-TNFα (min) 0 5 15 30 0 5 15 30
IP: α-Flag
TRADD
TNFR1
Input
TRADD
RIPK1
Tubulin
kDa
clap1/2-/-
Vehicle
Apt-1
Relative TRADD levels
Time (min)
i
clap1/2-/- + HA-mcIAP1
Vehicle
Apt-1
Flag-TNFα (min) 0 5 15 30 0 5 15 30
IP: α-Flag
TRADD
TNFR1
Input
TRADD
RIPK1
Tubulin
kDa
clap1/2-/- + HA-mcIAP1
Vehicle
Apt-1
Relative TRADD levels
Time (min)
j
Fadd deficient Jurkat
Ripk1 deficient Jurkat
DMSO
Vel
V+19
V+Nec1
V+NAC
V+zVAD
kDa
Caspase 8
Cleaved-Caspase 8
PARP
Cleaved-PARP
Actin
k
Jurkat
Fadd deficient
Ripk1 deficient
DMSO
Vel
V+Apt-1
V+Nec-1s
kDa
CC3
Tubulin

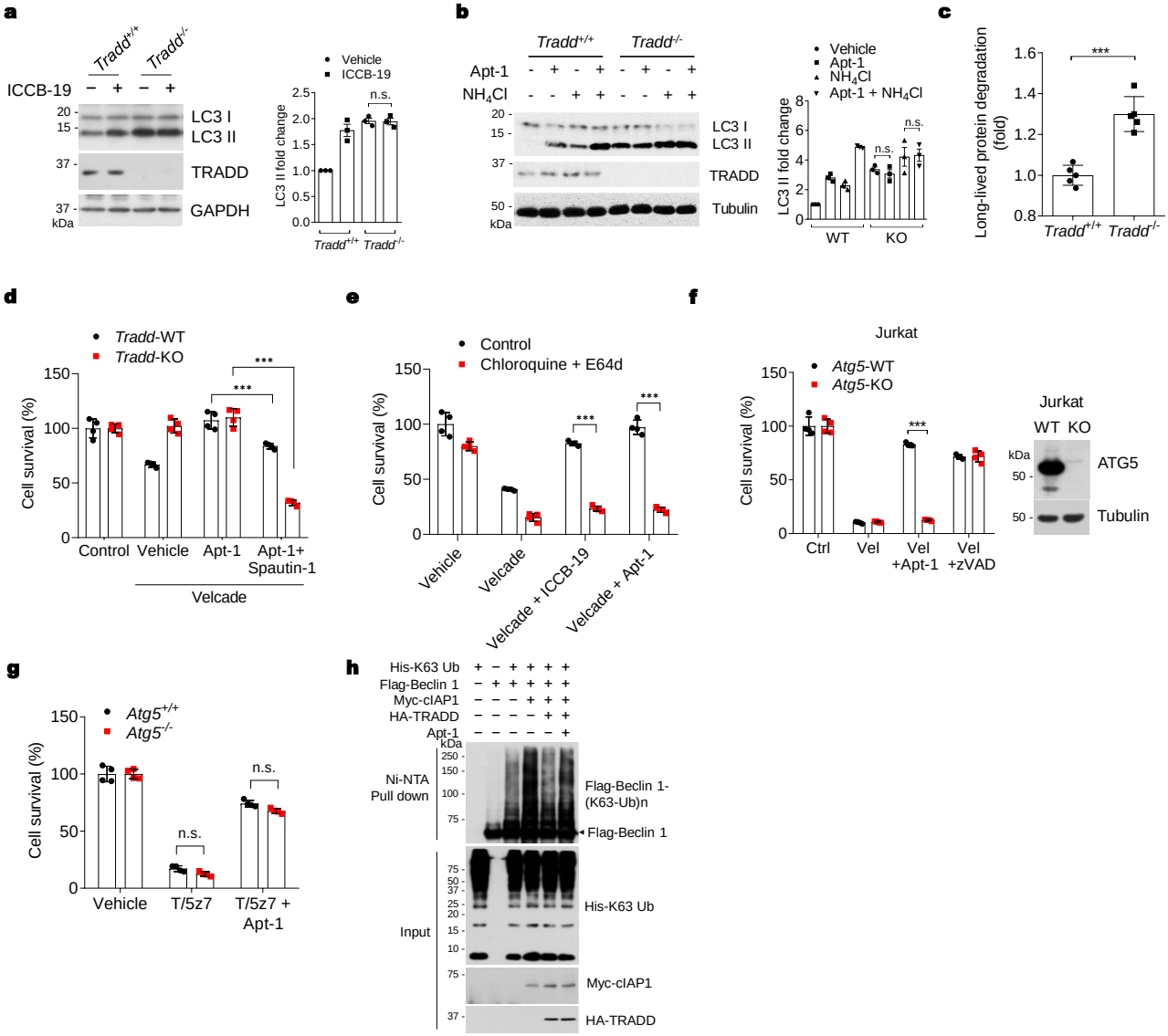
a
Tradd+/+
Tradd-/-
ICCB-19
LC3 I
LC3 II
TRADD
GAPDH
kDa
Vehicle
ICCB-19
LC3 II fold change
n.s.
b
Apt-1
NH4Cl
Tubulin
Vehicle
Apt-1
NH4Cl
Apt-1 + NH4Cl
WT
KO
c
Long-lived protein degradation (fold)
***
d
Tradd-WT
Tradd-KO
Cell survival (%)
Control
Vehicle
Apt-1
Apt-1+ Spautin-1
Velcade
e
Control
Chloroquine + E64d
Velcade
Velcade + ICCB-19
Velcade + Apt-1
f
Jurkat
Atg5-WT
Atg5-KO
Ctrl
Vel
Vel +Apt-1
Vel +zVAD
ATG5
g
Atg5+/+
Atg5-/-
T/5z7
T/5z7 + Apt-1
h
His-K63 Ub
Flag-Beclin 1
Myc-cIAP1
HA-TRADD
Apt-1
Ni-NTA Pull down
Flag-Beclin 1-(K63-Ub)n
Input
His-K63 Ub
Myc-cIAP1
HA-TRADD

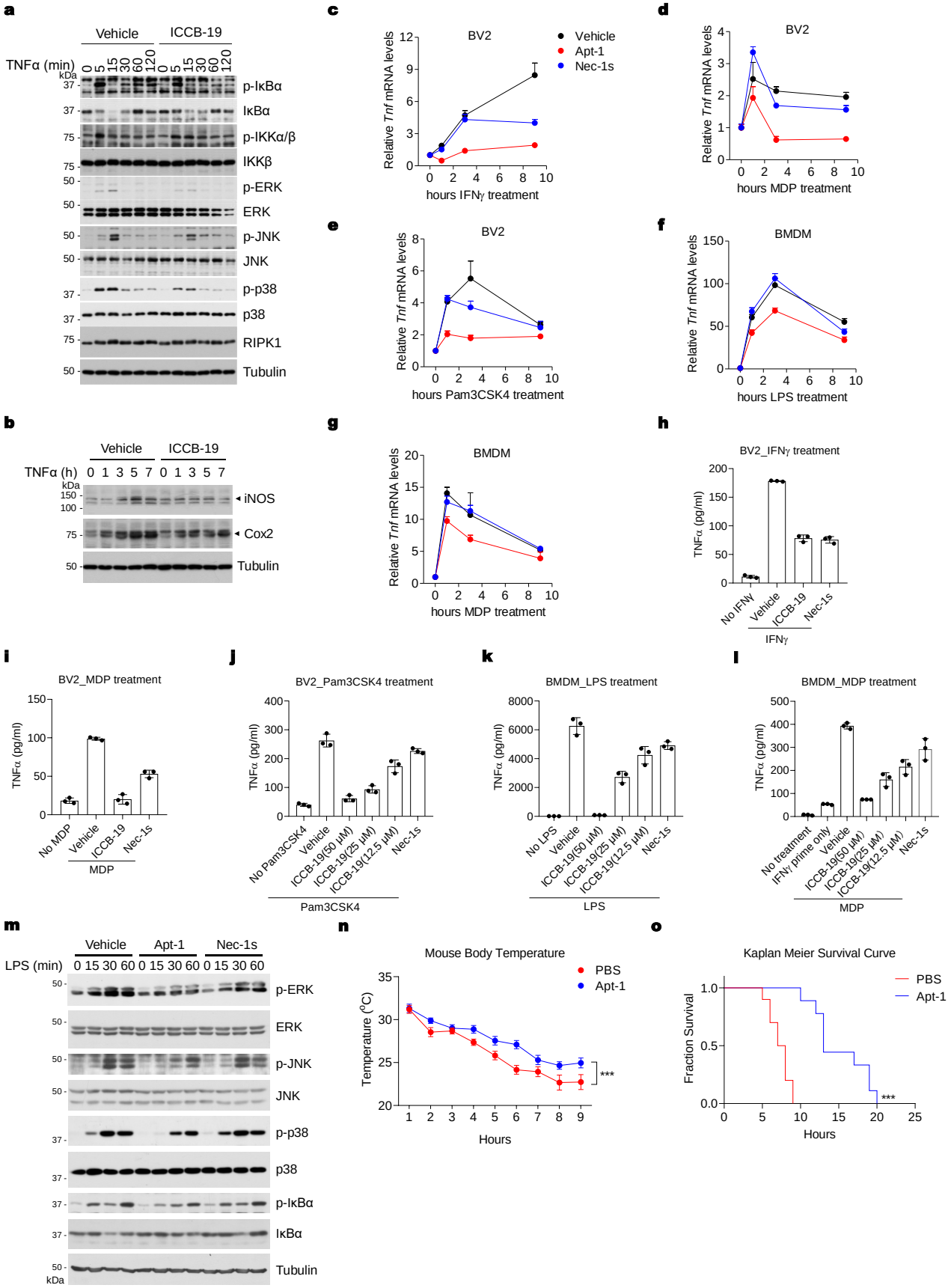
a
Vehicle
ICCB-19
TNFα (min)
0 5 15 30 60 120 0 5 15 30 60 120
kDa
p-IκBα
IκBα
p-IKKα/β
IKKβ
p-ERK
ERK
p-JNK
JNK
p-p38
p38
RIPK1
Tubulin
b
Vehicle
ICCB-19
TNFα (h) 0 1 3 5 7 0 1 3 5 7
iNOS
Cox2
Tubulin
c
BV2
Vehicle
Apt-1
Nec-1s
Relative Tnf mRNA levels
hours IFNγ treatment
d
BV2
hours MDP treatment
e
BV2
hours Pam3CSK4 treatment
f
BMDM
hours LPS treatment
g
BMDM
hours MDP treatment
h
BV2_IFNγ treatment
TNFα (pg/ml)
No IFNγ
Vehicle
ICCB-19
Nec-1s
IFNγ
i
BV2_MDP treatment
No MDP
MDP
j
BV2_Pam3CSK4 treatment
No Pam3CSK4
ICCB-19(50 μM)
ICCB-19(25 μM)
ICCB-19(12.5 μM)
Pam3CSK4
k
BMDM_LPS treatment
No LPS
LPS
l
BMDM_MDP treatment
No treatment
IFNγ prime only
m
Vehicle
Apt-1
Nec-1s
LPS (min) 0 15 30 60 0 15 30 60 0 15 30 60
p-ERK
ERK
p-JNK
JNK
p-p38
p38
p-IκBα
IκBα
Tubulin
n
Mouse Body Temperature
PBS
Apt-1
Temperature (°C)
Hours
***
o
Kaplan Meier Survival Curve
Fraction Survival
***

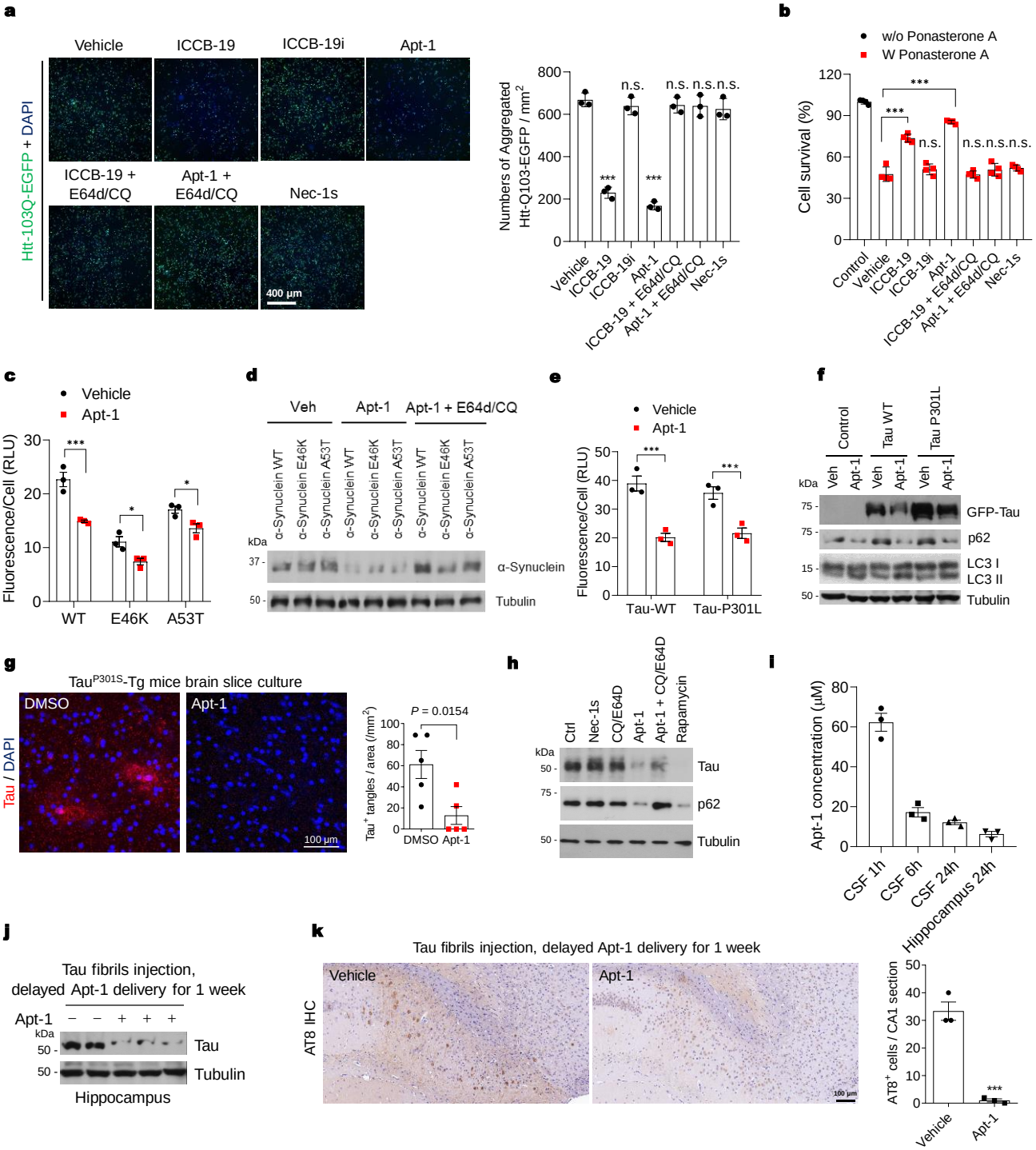
a
Vehicle
ICCB-19
ICCB-19i
Apt-1
ICCB-19 + E64d/CQ
Apt-1 + E64d/CQ
Nec-1s
Htt-103Q-EGFP + DAPI
400 μm
Numbers of Aggregated Htt-Q103-EGFP / mm²
n.s.
***
Vehicle
ICCB-19
ICCB-19i
Apt-1
ICCB-19 + E64d/CQ
Apt-1 + E64d/CQ
Nec-1s
b
w/o Ponasterone A
W Ponasterone A
Cell survival (%)
Control
c
Vehicle
Apt-1
Fluorescence/Cell (RLU)
WT
E46K
A53T
d
Veh
Apt-1
Apt-1 + E64d/CQ
α-Synuclein WT
α-Synuclein E46K
α-Synuclein A53T
kDa
α-Synuclein
Tubulin
e
Tau-WT
Tau-P301L
f
Control
Tau WT
Tau P301L
GFP-Tau
p62
LC3 I
LC3 II
Tubulin
g
Tau^P301S-Tg mice brain slice culture
DMSO
Apt-1
Tau / DAPI
100 μm
P = 0.0154
Tau⁺ tangles / area (/mm²)
h
Ctrl
Nec-1s
CQ/E64D
Apt-1 + CQ/E64D
Rapamycin
Tau
p62
Tubulin
i
Apt-1 concentration (μM)
CSF 1h
CSF 6h
CSF 24h
Hippocampus 24h
j
Tau fibrils injection, delayed Apt-1 delivery for 1 week
Hippocampus
k
Tau fibrils injection, delayed Apt-1 delivery for 1 week
AT8 IHC
AT8⁺ cells / CA1 section

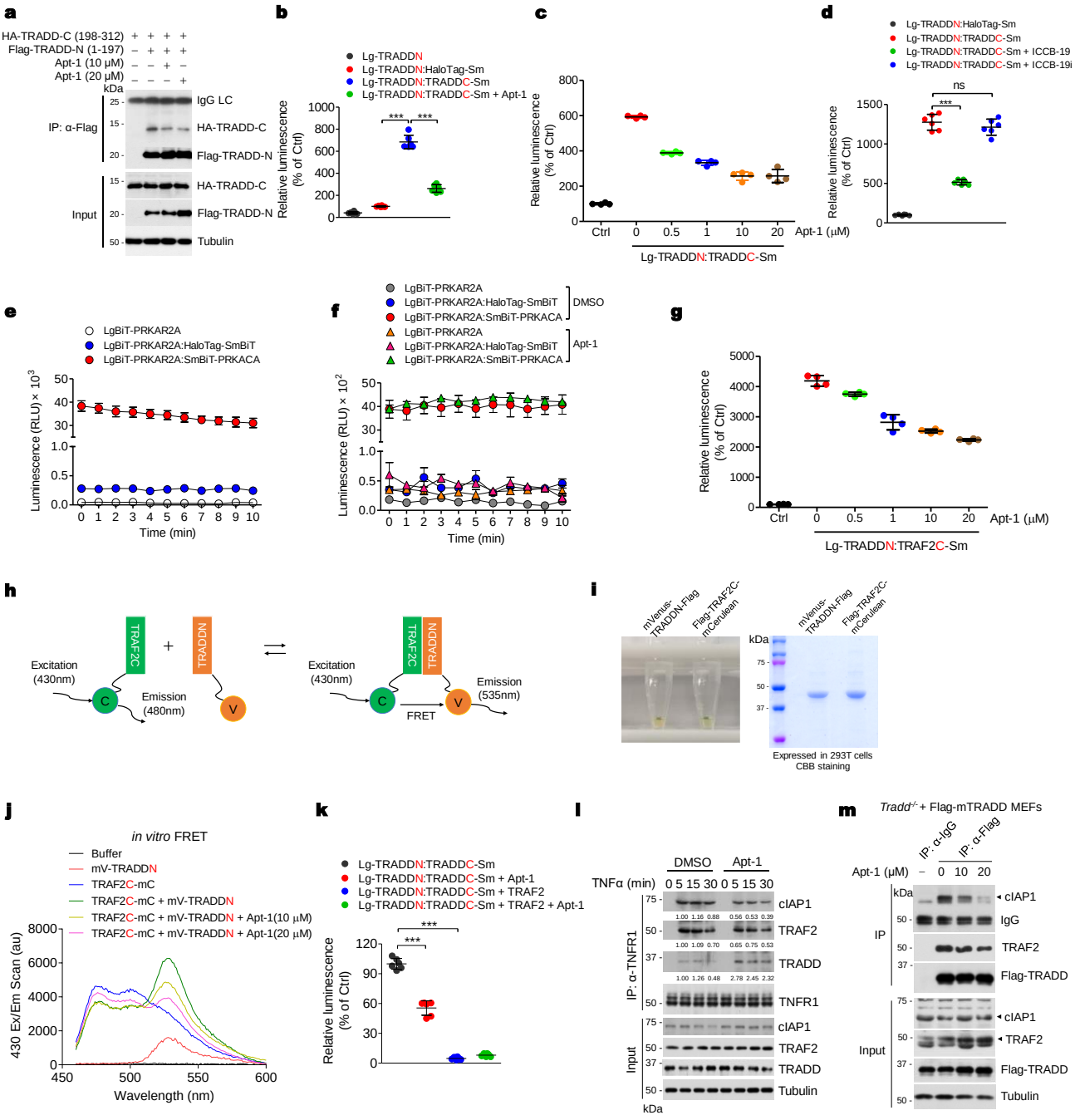
a
HA-TRADD-C (198-312)
Flag-TRADD-N (1-197)
Apt-1 (10 μM)
Apt-1 (20 μM)
kDa
IP: α-Flag
IgG LC
HA-TRADD-C
Flag-TRADD-N
Input
HA-TRADD-C
Flag-TRADD-N
Tubulin
b
Lg-TRADDN
Lg-TRADDN:HaloTag-Sm
Lg-TRADDN:TRADDC-Sm
Lg-TRADDN:TRADDC-Sm + Apt-1
Relative luminescence (% of Ctrl)
c
Relative luminescence (% of Ctrl)
Ctrl
Apt-1 (μM)
Lg-TRADDN:TRADDC-Sm
d
Lg-TRADDN:HaloTag-Sm
Lg-TRADDN:TRADDC-Sm
Lg-TRADDN:TRADDC-Sm + ICCB-19
Lg-TRADDN:TRADDC-Sm + ICCB-19l
ns
Relative luminescence (% of Ctrl)
e
LgBiT-PRKAR2A
LgBiT-PRKAR2A:HaloTag-SmBiT
LgBiT-PRKAR2A:SmBiT-PRKACA
Luminescence (RLU) × 10^3
Time (min)
f
LgBiT-PRKAR2A
LgBiT-PRKAR2A:HaloTag-SmBiT
LgBiT-PRKAR2A:SmBiT-PRKACA
DMSO
Apt-1
Luminescence (RLU) × 10^2
Time (min)
g
Relative luminescence (% of Ctrl)
Ctrl
Apt-1 (μM)
Lg-TRADDN:TRAF2C-Sm
h
TRAF2C
TRADDN
Excitation (430nm)
Emission (480nm)
Excitation (430nm)
Emission (535nm)
FRET
i
mVenus-TRADDN-Flag
Flag-TRAF2C-mCerulean
kDa
Expressed in 293T cells
CBB staining
j
in vitro FRET
Buffer
mV-TRADDN
TRAF2C-mC
TRAF2C-mC + mV-TRADDN
TRAF2C-mC + mV-TRADDN + Apt-1(10 μM)
TRAF2C-mC + mV-TRADDN + Apt-1(20 μM)
430 Ex/Em Scan (au)
Wavelength (nm)
k
Lg-TRADDN:TRADDC-Sm
Lg-TRADDN:TRADDC-Sm + Apt-1
Lg-TRADDN:TRADDC-Sm + TRAF2
Lg-TRADDN:TRADDC-Sm + TRAF2 + Apt-1
Relative luminescence (% of Ctrl)
l
DMSO
Apt-1
TNFα (min)
0 5 15 30 0 5 15 30
IP: α-TNFR1
cIAP1
TRAF2
TRADD
TNFR1
Input
cIAP1
TRAF2
TRADD
Tubulin
kDa
m
Tradd-/- + Flag-mTRADD MEFs
IP: α-IgG
IP: α-Flag
Apt-1 (μM)
IP
cIAP1
IgG
TRAF2
Flag-TRADD
Input
cIAP1
TRAF2
Flag-TRADD
Tubulin

Extended Data Figure 10

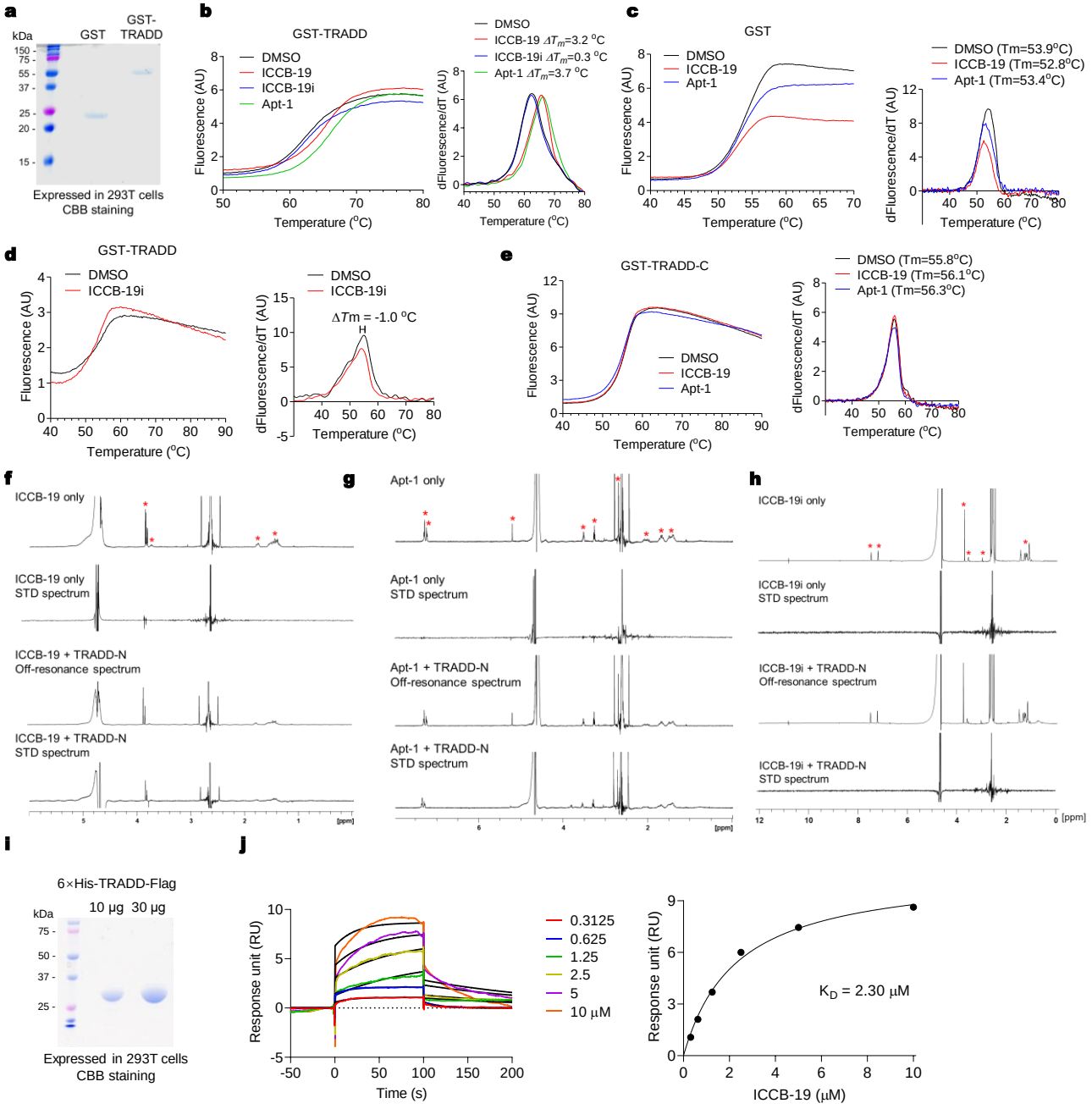

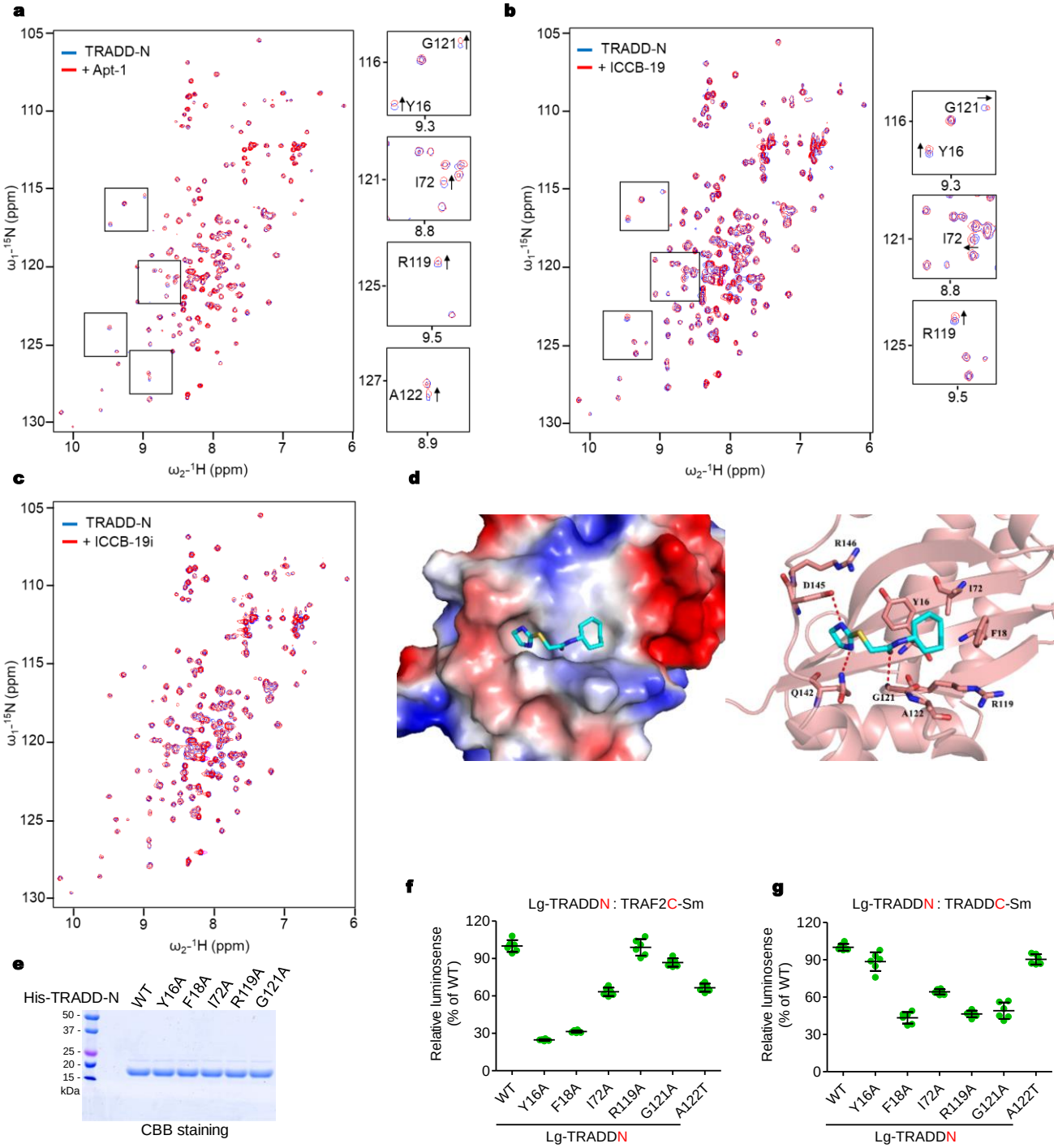
a
TRADD-N
+ Apt-1
G121
Y16
I72
R119
A122
b
TRADD-N
+ ICCB-19
c
TRADD-N
+ ICCB-19i
d
R146
D145
Y16
I72
F18
Q142
G121
A122
R119
e
His-TRADD-N
WT
Y16A
F18A
I72A
R119A
G121A
kDa
CBB staining
f
Lg-TRADDN : TRAF2C-Sm
Relative luminosense (% of WT)
Lg-TRADDN
g
Lg-TRADDN : TRADDC-Sm
Relative luminosense (% of WT)
Lg-TRADDN

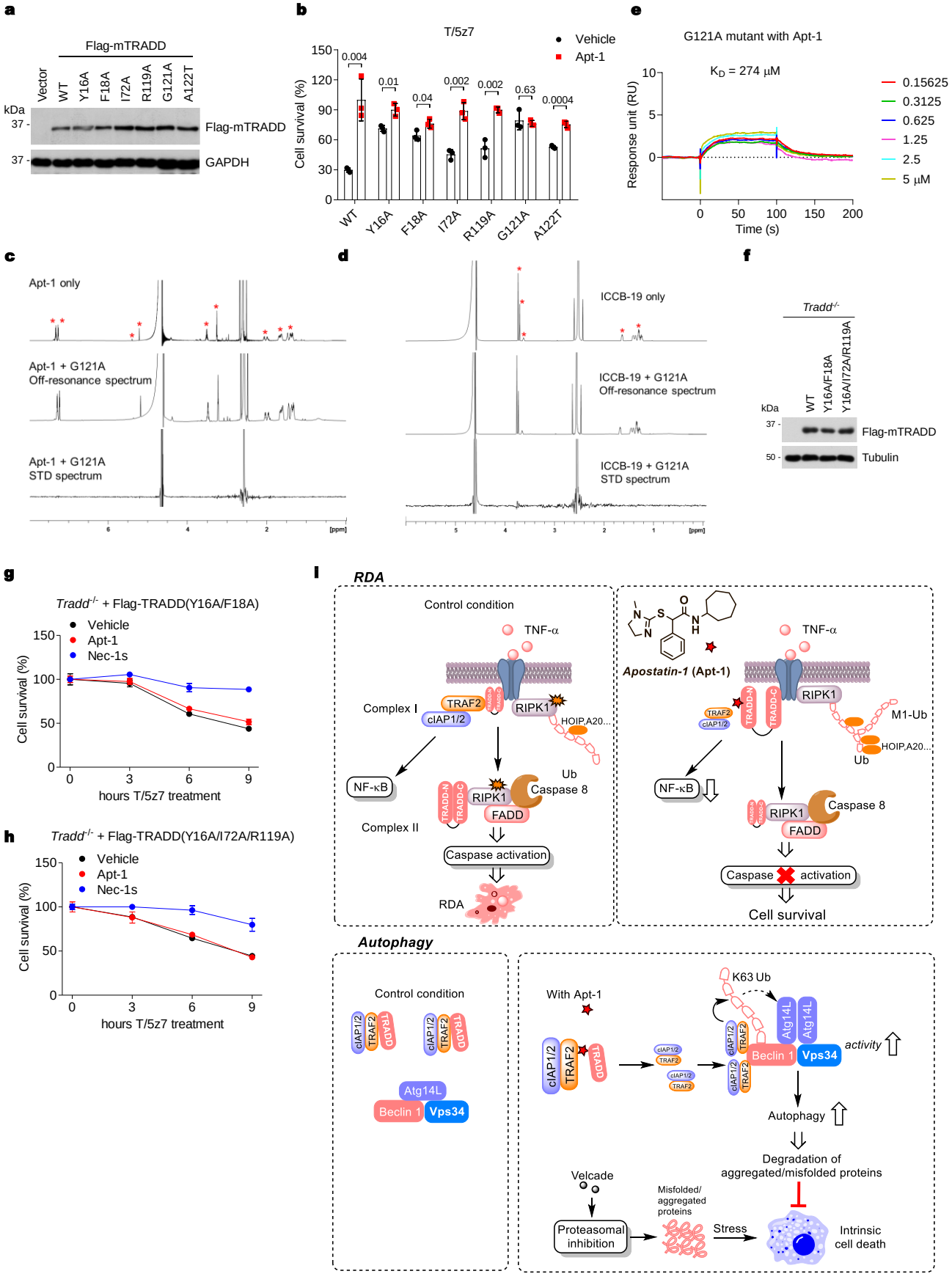
a
Flag-mTRADD
Vector
WT
Y16A
F18A
I72A
R119A
G121A
A122T
kDa
37 -
Flag-mTRADD
37 -
GAPDH
b
T/5z7
Vehicle
Apt-1
Cell survival (%)
0.004
0.01
0.04
0.002
0.002
0.63
0.0004
WT
Y16A
F18A
I72A
R119A
G121A
A122T
e
G121A mutant with Apt-1
K_D = 274 μM
Response unit (RU)
Time (s)
0.15625
0.3125
0.625
1.25
2.5
5 μM
c
Apt-1 only
Apt-1 + G121A
Off-resonance spectrum
Apt-1 + G121A
STD spectrum
[ppm]
d
ICCB-19 only
ICCB-19 + G121A
Off-resonance spectrum
ICCB-19 + G121A
STD spectrum
[ppm]
f
Tradd-/-
WT
Y16A/F18A
Y16A/I72A/R119A
kDa
37 -
Flag-mTRADD
50 -
Tubulin
g
Tradd-/- + Flag-TRADD(Y16A/F18A)
Vehicle
Apt-1
Nec-1s
Cell survival (%)
hours T/5z7 treatment
h
Tradd-/- + Flag-TRADD(Y16A/I72A/R119A)
Vehicle
Apt-1
Nec-1s
Cell survival (%)
hours T/5z7 treatment
i
RDA
Control condition
TNF-α
Complex I
TRAF2
cIAP1/2
RIPK1
HOIP,A20...
Ub
NF-κB
Caspase 8
Complex II
TRADD-N
TRADD-C
RIPK1
FADD
Caspase activation
RDA
Apostatin-1 (Apt-1)
TNF-α
RIPK1
M1-Ub
HOIP,A20...
Ub
NF-κB
Caspase 8
RIPK1
FADD
Caspase activation
Cell survival
Autophagy
Control condition
cIAP1/2
TRAF2
TRADD
Atg14L
Beclin 1
Vps34
With Apt-1
K63 Ub
activity
Autophagy
Degradation of
aggregated/misfolded proteins
Velcade
Proteasomal
inhibition
Misfolded/
aggregated
proteins
Stress
Intrinsic
cell death